

Afford-X: Generalizable and Slim Affordance Reasoning for Task-oriented Manipulation

Xiaomeng Zhu^{*} , Yuyang Li^{*} , Leyao Cui , Pengfei Li ,
Huan-ang Gao , Yixin Zhu , and Hao Zhao 

Abstract—Object affordance reasoning, the ability to infer object functionalities based on physical properties, is fundamental for task-oriented planning and activities in both humans and Artificial Intelligence (AI). This capability, required for planning and executing daily activities in a task-oriented manner, relies on commonsense knowledge of object physics and functionalities, extending beyond simple object recognition. Current computational models for affordance reasoning from perception lack generalizability, limiting their applicability in novel scenarios. Meanwhile, comprehensive Large Language Models (LLMs) with emerging reasoning capabilities are challenging to deploy on local devices for task-oriented manipulations. Here, we introduce LVIS-Aff, a large-scale dataset comprising 1,496 tasks and 119k images, designed to enhance the generalizability of affordance reasoning from perception. Utilizing this dataset, we develop Afford-X, an end-to-end trainable affordance reasoning model that incorporates Verb Attention and Bi-Fusion modules to improve multi-modal understanding. This model achieves up to a 12.1% performance improvement over the best-reported results from non-LLM methods, while also demonstrating a 1.2% enhancement compared to our previous conference paper. Additionally, it maintains a compact 187M parameter size and infers nearly 50 times faster than the GPT-4V API. Our work demonstrates the potential for efficient, generalizable affordance reasoning models that can be deployed on local devices for task-oriented manipulations. We showcase Afford-X’s effectiveness in enabling task-oriented manipulations for robots across various tasks and environments, underscoring its efficiency and broad implications for advancing robotics and AI systems in real-world applications.

Index Terms—Affordance reasoning, task-oriented manipulation, slim, generalizable.

Manuscript received January x, 2025; revised x x, 2025. This work was supported in part by the National Science and Technology Major Project (Grant 2022ZD0114900), the National Natural Science Foundation of China (Grant 62376031), the Beijing Nova Program, the State Key Lab of General AI at Peking University, the PKU-BingJi Joint Laboratory for Artificial Intelligence, and the National Comprehensive Experimental Base for Governance of Intelligent Society, Wuhan East Lake High-Tech Development Zone. (Corresponding authors: Yixin Zhu; Hao Zhao.)

Xiaomeng Zhu, Yuyang Li, Leyao Cui, and Yixin Zhu are with the Institute for Artificial Intelligence, Peking University, Beijing 100091, China (email: xiaomeng.zhu@connect.ust.hk, y.li@stu.pku.edu.cn, cuileiyao24@mails.ucas.ac.cn, yixin.zhu@pku.edu.cn).

Xiaomeng Zhu is also with the Department of Computer Science and Engineering, Hong Kong University of Science and Technology, Hong Kong 999077, China.

Leyao Cui is also with Shenyang Institute of Automation, Chinese Academy of Sciences, Shenyang 110016, China.

Pengfei Li and Hao Zhao are with the Institute for AI Industry Research, Tsinghua University, Beijing 100084, China (li-pf22@mails.tsinghua.edu.cn, zhaohao@air.tsinghua.edu.cn).

Huan-ang Gao is with the Department of Computer Science, Tsinghua University, Beijing 100084, China (gha24@mails.tsinghua.edu.cn).

Implementable code is available at: <https://zhuxmmm.github.io/Afford-X>

^{*} Equal contribution.

I. INTRODUCTION

EFFECTIVE interaction with the world demands more than object recognition; it requires understanding how objects can be used. This concept, known as *affordance reasoning* [1], [2], transcends the traditional “what is where” paradigm [3] of object detection and classification systems [4]–[8]. Through affordance reasoning, agents infer potential functions from physical properties—a fundamental capability that enables both task-oriented manipulation and adaptive problem-solving in complex environments [9], [10].

This reasoning capability enables humans to naturally select appropriate tools for specific tasks [11] and devise creative solutions in unfamiliar or resource-constrained environments [12]. Consider, for example, repurposing a hollowed-out bell pepper as a water container when conventional containers are unavailable, as shown in Fig. 1(c). Such adaptability, rooted in understanding object properties and their potential functions, exemplifies the flexibility required for effective interaction across diverse environments [13].

The importance of affordance reasoning extends beyond human cognition into AI and robotics [2], [14]. In task-oriented manipulation [15]–[19], agents must process both task requirements (textual input) and environmental perception (visual input) to select and use appropriate objects for specific goals. This process requires reasoning about feature cues and matching them to novel task contexts [20], as illustrated in Figs. 2a and 2b. Developing robust affordance reasoning capabilities could significantly enhance AI systems’ ability to operate flexibly in complex, real-world environments [21].

Despite the significant benefits of affordance reasoning, its computational implementation faces several key challenges, particularly in designing frameworks suitable for local deployment and offline processing. Robotic platforms typically operate under strict computational constraints—whether using NVIDIA’s Jetson Orin development board or even high-end RTX 4090 GPUs with 24GB memory [22]. These limitations prevent the deployment of large-scale pre-trained generative Multimodal Large Language Models (MLLMs) [23] due to computing capabilities, power constraints, usage policies, and information security concerns [24], [25]. While smaller pre-trained generative MLLMs like SPHINX 1.1B [26] can operate locally, their limited knowledge bases and reasoning capabilities prove insufficient for complex affordance reasoning. In contrast, pre-trained Multimodal Models (MMs) [4], [27]–[31] achieve superior performance with fewer parameters and faster response times, likely because they leverage knowledge



Fig. 1: **Affordance reasoning for task-oriented manipulation.** Afford-X provides efficient visual affordance reasoning through: (a) two comprehensive datasets—COCO-Aff (112k images, 1,144 tasks, 80 categories) and LVIS-Aff (119k images, 1,496 tasks, 1,064 categories); (b) real-time processing (2.38 Frames Per Second (FPS)) with a compact 187M-parameter architecture generating bounding boxes and object masks; (c) robust generalization demonstrated through task-specific object selection and multi-object identification at 0.7 confidence threshold; (d) integration with robotic systems for simulated task-oriented manipulation.

directly from the image feature space, capturing fine-grained visual details essential for affordance reasoning [32].

Training these slim MMs presents additional challenges, particularly when pre-training techniques ignore the fundamental nature of affordance. Models trained directly on object detection datasets often develop biased understanding, over-emphasizing familiar nouns. This bias can lead to failures when task descriptions include prominently visible objects, as the model may misinterpret an affordance reasoning task as simple object detection. For example, given the task “*clean bottle with*,” a model might fixate on detecting “*bottle*” while missing the critical action “*clean*,” failing to understand the task’s true intent (see Figs. 2c and 2d). Moreover, some pre-trained MMs, such as Multimodal DEtection TRansformer (MDETR) [4], rely on simple concatenation of visual and language features, potentially limiting their comprehension of multimodal data.

Developing slim models with accurate and generalized affordance understanding requires both a large-scale corpus and diverse knowledge representation [33]. This diversity depends on three critical dimensions: the range of tasks, the quantity of images, and the variety of target object categories. Deficiencies in any of these dimensions can limit a robot’s ability to make contextual decisions when encountering dynamic affordances, diverse layouts, and novel objects [2], [32], [34]. However, expanding this knowledge base presents unique challenges due to the complex many-to-many mapping between affordance tasks and target objects—unlike the straightforward one-to-one relationships in object detection [35], [36]. A single object can serve multiple tasks, and conversely, one task might be accomplished using various objects (see Fig. 3) [37]. Despite

previous efforts involving manual annotations [37]–[39] or LLMs, creating truly diverse affordance reasoning datasets remains a significant challenge [17].

To address these challenges, we propose Afford-X, a slim end-to-end multimodal reasoning framework built on a knowledge distillation architecture inspired by TOIST [15]. Our framework consists of paired teacher and student models sharing the same architecture. It processes text-based task descriptions and visual scene inputs to autonomously identify appropriate objects for given tasks, producing both detection bounding boxes and fine-grained segmentation masks (see Fig. 1(b)). The training process occurs in two stages: first, the teacher model learns in an oracle manner using target object category labels in the text input; then, this knowledge transfers to the student model, which operates without such labels. This distillation approach proves particularly effective for scenarios with size constraints, as the student model’s architecture can adapt to practical requirements while maintaining effective supervision from the teacher.

To enhance our framework’s capabilities, we introduce two key modules. The Verb Attention (VA) module emphasizes action words in the input, ensuring accurate task understanding rather than mere object recognition. The Bi-Fusion (BF) module, inspired by BLIP [40], improves upon simple feature concatenation methods to better capture complex interactions between visual and textual information. Our experimental results (see Fig. 11) demonstrate that Afford-X, despite its compact 187M parameters, outperforms even GPT-4V in affordance reasoning tasks while achieving real-time inference speeds of 2.38 FPS—making it practical for real-world deployment.

To strengthen Afford-X’s generalization capabilities, we de-

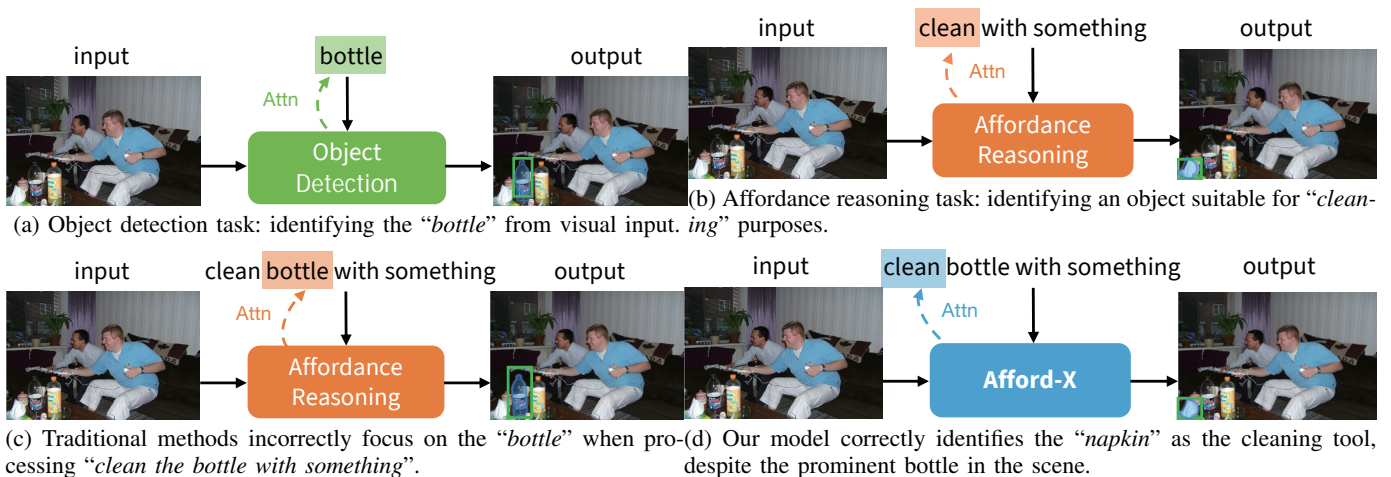


Fig. 2: **Affordance reasoning for task-oriented manipulation.** Afford-X provides efficient visual affordance reasoning through comprehensive datasets and real-time processing. (a) We introduce two new datasets that expand the knowledge base: COCO-Aff (112k images, 1,144 tasks, 80 categories) and LVIS-Aff (119k images, 1,496 tasks, 1,064 categories). (b) Our model processes inputs in real-time at 2.38 FPS using a compact 187M-parameter architecture to generate bounding boxes and object masks. (c) The system demonstrates robust generalization through task-specific object selection and identifies multiple suitable objects at a 0.7 confidence threshold. (d) The framework integrates with robotic systems to enable task-oriented manipulation in simulated environments.

veloped an automated pipeline that leverages LLMs to convert object detection datasets into affordance reasoning datasets. This pipeline employs GPT-4 in dual roles: as a producer generating task-object pairs from object categories, and as a quality inspector filtering out errors and inconsistencies. Using this approach, we created two comprehensive datasets: COCO-Aff from COCO2014 [35] and LVIS-Aff from LVIS [36]. COCO-Aff features 1,144 diverse tasks, 112k training images, and 80 object categories, while LVIS-Aff expands to 1,494 tasks, 119k images, and 1,064 object categories, offering broader coverage of both indoor and outdoor scenarios (see Fig. 1(a)). Models trained on these datasets show significant improvements in generalization, with accuracy gains of 22.9% and 24.7% respectively on unseen tasks.

We validate these improvements through extensive testing of Afford-X’s ability to support embodied agents in diverse physical environments. Beyond evaluations on natural images from datasets like COCO [35], we utilize textured meshes from Objaverse [41] and OmniGibson [42] to create scenes with diverse, randomly placed objects rendered using photorealistic ray-tracing, as shown in Fig. 1(d). This approach enables assessment of our model’s robustness to complex object geometry, appearance variations, and challenging environmental conditions including clustered objects, varying lighting, and visual distractions. We further demonstrate practical applicability through simulated object collection tasks, where Afford-X integrates with standard grasp planners and motion planners on a mobile manipulator to perceive scenes, select appropriate objects, and execute retrieval actions.

This article significantly extends our previous TOIST work [15] through several key contributions:

- Development of knowledge distillation-based Afford-X with innovative VA and BF modules, enhancing action recognition and multimodal interpretation capabilities
- Creation of comprehensive affordance reasoning datasets: COCO-Aff and its expanded version LVIS-Aff

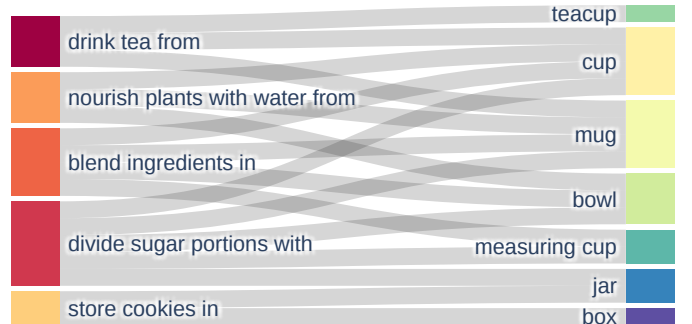


Fig. 3: **Task-object mapping in affordance reasoning.** Affordance reasoning involves complex many-to-many relationships between tasks and objects. (a) We visualize task descriptions from LVIS-Aff on the left and their compatible object categories on the right. (b) The connections demonstrate how individual tasks can be accomplished with multiple objects. (c) The mapping reveals how single objects can serve multiple different tasks, highlighting the complexity of affordance relationships.

- Extensive validation demonstrating significant performance improvements over our previous approach, particularly in dynamic environments and task-oriented manipulation scenarios

The paper continues with a comprehensive review of related work (Sec. II), followed by detailed descriptions of our dataset construction (Sec. IV), model architecture (Sec. III), and embodied affordance reasoning approach (Sec. V). We present experimental results in Sec. VI, discuss task-oriented manipulation findings in Sec. VI-F, and conclude with key insights in Sec. VII.

II. RELATED WORK

In this section, we review three key aspects of affordance research: learning-based affordance reasoning (Sec. II-A), datasets for training and evaluation (Sec. II-B), and task-oriented manipulation approaches (Sec. II-C), examining how

robots adapt their strategies based on goals and object interactions.

A. Learning-based Affordance Reasoning

The concept of affordance, introduced by American psychologist James J. Gibson [1], proposes that environmental objects inherently offer action possibilities—for instance, a chair affords sitting. This fundamental notion, which emphasizes the relationship between physical properties and potential functions, has become central to how robots understand and interact with their environment [2].

As affordance research entered the computer vision domain, early approaches focused on establishing direct mappings between visual features and potential actions, bypassing explicit object recognition [43]. These traditional methods combined handcrafted features—including shape, size, texture, color, and material—with Bayesian networks [44] or support vector machines [45] to encode relationships between geometric features and affordances [46]–[48]. However, these approaches struggled to generalize across diverse object appearances and environmental contexts [49].

The emergence of deep learning transformed affordance reasoning through its powerful feature extraction capabilities. These models leverage multi-layer networks and large-scale datasets to capture rich object features and learn affordance cues, achieving enhanced performance and robustness [50]. Their success in identifying functional regions—such as graspable or supportable areas—has significantly advanced robotic task-oriented manipulation [43], [50]–[52]. However, challenges persist in capturing contextual dependencies and complex semantic relationships, particularly in cluttered scenes with multiple interacting objects.

The integration of semantic information with visual cues marked the next major advance. Modern models leverage category-level knowledge for object function inference, enabling more effective task-oriented object detection [15], [53]. This enhanced contextual understanding provides deeper insights into object-environment interactions [4], [15], [54]–[56]. Transformer-based architectures, especially vision-language pre-training models [4], [27]–[31], have further advanced the field through sophisticated cross-modal alignment techniques. These approaches demonstrate superior flexibility and generalizability compared to traditional Convolutional Neural Network (CNN)-based methods, particularly in complex and dynamic scenarios.

Most recently, the rich commonsense knowledge embedded in LLMs has opened new possibilities for affordance reasoning. CoTDet demonstrates this potential through structured task decomposition [57], while AffordanceLLM enhances open-world inference by combining visual perception with LLM capabilities [32]. However, deploying large-scale LLMs like GPT-4 presents significant challenges for robotic platforms that require local, offline inference. While small-scale LLMs offer an alternative, they struggle with limited knowledge bases and reasoning capabilities—particularly in sparse language spaces compared to dense image feature spaces [58]. To address these limitations, we propose Afford-X, a MM-

based end-to-end framework inspired by TOIST [15]. Our approach achieves efficient inference with compact parameters, enabling broader deployment across manipulation platforms.

B. Dataset for Affordance Reasoning

The proliferation of deep learning in affordance reasoning has highlighted datasets as a critical foundation for model development. A dataset’s effectiveness depends on three key dimensions: the diversity of tasks, the quantity of images, and the range of object categories. Tab. I summarizes the major datasets in this field. The first significant milestone came from Myers *et al.* [59], who introduced both a framework for joint affordance localization and recognition and the field’s first pixel-level annotated dataset. While groundbreaking, this initial dataset focused primarily on surface features, overlooking the crucial role of human-object interactions in affordance reasoning. Chuang *et al.* [39] addressed this limitation with the ADE-Affordance dataset, built upon ADE20K [38], incorporating both physical constraints and social norms to better align with real-world reasoning challenges.

TABLE I: **Comparison of affordance detection datasets.** We analyze the key characteristics of major datasets in affordance reasoning. (a) We evaluate datasets based on their number of images (#Imgs), object categories (#Cats), and affordance/task categories (#Aff). (b) Each dataset builds upon different source datasets, providing varying foundations for affordance learning. (c) Our proposed datasets, COCO-Aff and LVIS-Aff, achieve significant expansion across all three dimensions compared to existing work.

Dataset	#Imgs	#Cats	#Aff	Source
ADE-Aff [39]	1000	150	7	ADE20K [38]
PAD [60]	4002	72	31	\
PADv2 [61]	30000	103	39	\
PAD-L [61]	4002	72	31	\
COCO-Tasks [37]	39724	49	14	COCO2024 [35]
RIO [17]	40214	69	>100	COCO2024
COCO-Aff	112k	80	1144	COCO2024
LVIS-Aff	119k	1064	1496	LVIS [36]

Recognizing that affordances fundamentally connect to human behavioral goals—reflecting Gibson’s concept of animal-environment complementarity—researchers began developing goal-oriented datasets. Luo *et al.* pioneered this direction with PAD [60] and its successor PADv2 [62], explicitly modeling the relationship between human goals and affordances while encompassing more complex scenarios. Lu *et al.* [61] further advanced this approach through PAD-L, which integrated natural language in affordance detection to enable object segmentation based on phrase-based affordance descriptions. However, their reliance on a limited affordance dictionary for paraphrasing constrained the capture of natural language complexity.

The field then shifted toward task-specific object selection. Sawatzky *et al.* [53] introduced the COCO-Task dataset, derived from COCO [63], marking the first transformation of an object detection dataset into an affordance reasoning dataset. While innovative, its scope remained limited by predefined 14 tasks and rigid phrase representations. Qu *et al.* [17] addressed these constraints with the RIO dataset, also built upon COCO2014, offering richer tasks and more diverse

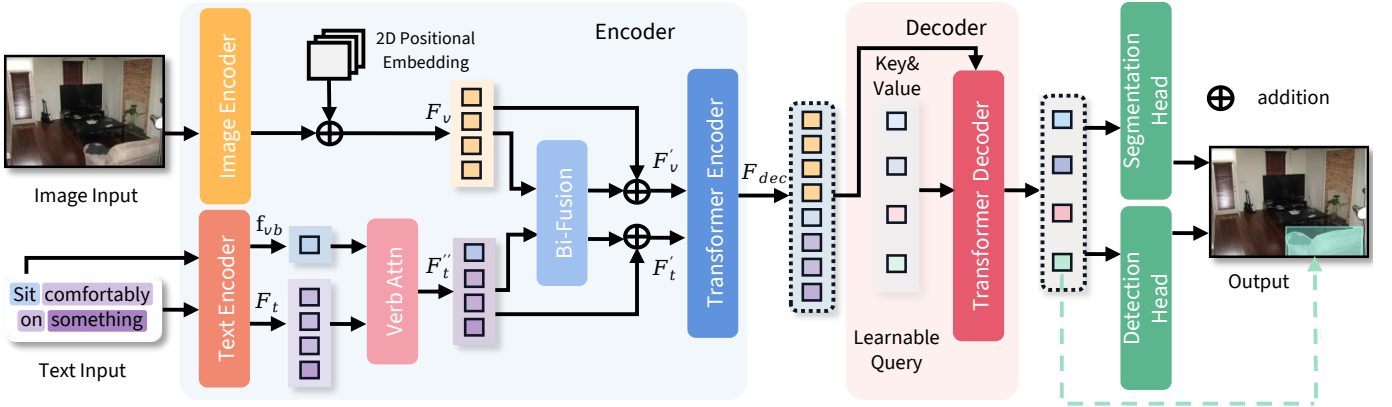


Fig. 4: **Architecture of the Afford-X.** Our framework processes visual and textual inputs through multiple specialized components. (a) The model begins by extracting visual features from images and textual features from prompts containing words like “something”. (b) The **Bi-Fusion module** performs bi-directional attention between visual and textual features to enhance multimodal understanding. (c) The **Verb Attn module** strengthens the model’s focus on action verbs to reduce category interference. (d) A Transformer encoder-decoder processes these enhanced features using learnable query vectors, producing parallel outputs for object detection and instance segmentation.

descriptions for broader scenario coverage. However, RIO’s limited object categories prove insufficient for dynamic open-world environments, and despite leveraging LLM for task construction, it still requires extensive human annotation for task-object pair filtering.

To overcome these limitations, we propose an automated pipeline for converting object detection datasets into affordance reasoning datasets. Our approach employs LLM in dual roles—as both producer and inspector—significantly reducing the need for human annotation. Through this pipeline, we have created COCO-Aff and LVIS-Aff, establishing new benchmarks in task coverage, image quantity, and object category diversity. These datasets provide models with a substantially richer knowledge base while maintaining data quality through automated verification, enabling more robust and generalizable affordance reasoning.

C. Task-oriented Manipulation

Ikeuchi and Hebert’s seminal work [64] established that vision systems should adapt their architectures to specific tasks rather than pursuing a general-purpose approach. This task-oriented vision paradigm has become fundamental to robotic manipulation, enabling systems to handle diverse tasks posed by algorithms or human users. These tasks span a broad spectrum—from object manipulation with varying grasp types [64]–[66] and purposes [2], [13], [19], [67] to complex environmental interactions such as door opening and water pouring [68]–[70]. At its core, task-oriented manipulation requires optimal system configuration through the selection of appropriate sensor signals [71], task representations [13], [65], [66], processing modules, and manipulation strategies [18], [19], [72], [73], all conditioned on specific goals and target objects.

Current task-oriented robotic vision and manipulation systems, however, typically operate under a significant constraint: they assume the suitable object for a task has already been specified. This limitation reduces system autonomy by requiring human input for object selection. Our approach addresses this fundamental gap by integrating affordance reasoning ca-

capabilities within scene understanding [74], enabling robots to actively reason about and select appropriate objects for given tasks. This integration represents a crucial step toward truly autonomous task-oriented manipulation systems that can adapt to diverse environments and task requirements.

III. THE AFFORD-X

This section presents our Afford-X framework for affordance reasoning. We begin with a formal problem formulation (Sec. III-A), followed by the model architecture (Sec. III-B), noun-pronoun distillation strategy (Sec. III-C), and key architectural components (Sec. III-D).

A. Problem Formulation

Given an RGB image $X_v \in \mathbb{R}^{3 \times H_0 \times W_0}$ and a task description X_l (e.g., “sit comfortably on”), our goal is to detect and segment objects most suitable for the specified task. The model predicts bounding boxes $B_{\text{pred}} = \{b_1, \dots, b_{n_{\text{pred}}}\}$, instance segmentation masks $M_{\text{pred}} = \{m_1, \dots, m_{n_{\text{pred}}}\}$, and preference scores $S_{\text{pred}} = \{\hat{s}_1, \dots, \hat{s}_{n_{\text{pred}}}\} \in [0, 1]^{n_{\text{pred}}}$. Each bounding box $b_i \in [0, 1]^4$ contains normalized center coordinates and dimensions, while preference scores indicate object suitability for the task. We denote the complete set of predictions as $O_{\text{pred}} = \langle B_{\text{pred}}, M_{\text{pred}}, S_{\text{pred}} \rangle$. Formally, we seek a function f such that:

$$f(X_v, X_l) = \langle B_{\text{pred}}, M_{\text{pred}}, S_{\text{pred}} \rangle. \quad (1)$$

B. Affordance Reasoning Model Architecture

To identify suitable objects without explicit object category labels, we design the Afford-X with parallel visual and textual pathways, enhanced by specialized modules for multimodal understanding (illustrated in Fig. 4). A pre-trained visual encoder processes the input image X_v to extract visual features F_v , while a text encoder processes the task description X_l to generate textual features F_t . Two key components enhance these representations: the **VA module** processes F_t to produce enhanced text features F'_t that emphasize task-specific actions, while the **BF module** integrates F'_t with F_v to generate fused

features F'_v and F'_t that capture fine-grained associations between vision and language.

The fused features pass through a transformer encoder-decoder architecture, where the encoder captures global relationships through self-attention mechanisms, and the decoder employs learnable query vectors to generate refined outputs. These outputs are projected through parallel heads to produce bounding boxes B_{pred} and segmentation masks M_{pred} . The decoder also outputs logits $\mathbf{G}_{\text{pred}} = [\hat{\mathbf{g}}_1, \dots, \hat{\mathbf{g}}_{n_{\text{pred}}}] \in \mathbb{R}^{n_{\text{pred}} \times n_{\text{max}}}$ for computing preference scores S_{pred} . To handle variable-length task descriptions, we pad inputs to length n_{max} (default 256) and include a special “no-object” class token for handling irrelevant predictions. For each predicted object i , the preference score $\hat{s}_i \in S_{\text{pred}}$ is computed as:

$$\hat{s}_i = 1 - \frac{\exp(\hat{g}_{n_{\text{max}}})}{\sum_{j=1}^{n_{\text{max}}} \exp(\hat{g}_j)}, \quad (2)$$

where \hat{g}_j^i represents the logit corresponding to the j -th text token for the i -th predicted object, and n_{max} includes both padding tokens and the “no-object” class token.

During training, we compute a bipartite matching between predicted and ground truth objects using the Hungarian algorithm [75]. The matched predictions are supervised with localization losses (L1 loss and Generalized Intersection over Union loss [76]) and segmentation losses (Dice/F-1 loss [77] and focal cross-entropy loss [78]). We incorporate the soft-token prediction loss and contrastive alignment loss from MDETR [4], adapting them to focus on the entire verb-pronoun description rather than individual tokens. The total loss for the Afford-X is formulated as:

$$\begin{aligned} \mathcal{L}_{\text{Afford-X}} = & \lambda_1 \mathcal{L}_{\text{L1}} + \lambda_2 \mathcal{L}_{\text{GIoU}} + \lambda_3 \mathcal{L}_{\text{Dice}} \\ & + \lambda_4 \mathcal{L}_{\text{Cross}} + \lambda_5 \mathcal{L}_{\text{Token}} + \lambda_6 \mathcal{L}_{\text{Align}}, \end{aligned} \quad (3)$$

where λ_1 to λ_6 are weights for the respective loss components.

C. Noun-Pronoun Distillation

To enable object inference without explicit category labels, we introduce a noun-pronoun distillation framework (illustrated in Fig. 5). Our approach uses a teacher model trained on task descriptions containing object labels (e.g., “sit comfortably with a couch”) and a student model that processes category-free descriptions (e.g., “sit comfortably with something”). Through clustering and preference distillation, the teacher transfers its object-centric knowledge to the student.

Clustering Distillation: We maintain a text feature memory bank that stores noun features from the teacher model, enabling the student to select appropriate noun prototypes for pronoun replacement. The process operates on enhanced text features F'_{noun} and F'_{pron} , corresponding to noun and pronoun tokens after VA module processing.

The memory bank is structured as a $n_{\text{task}} \times n_{\text{mem}} \times d$ tensor, where n_{task} represents the number of tasks, n_{mem} is the per-task memory size, and d is the feature dimension. For each task j , we maintain a queue $\mathbf{F}_{\text{mem}}^j = [F_1^j, F_2^j, \dots, F_{n_{\text{mem}}}^j]$ of noun features. During training, we update this queue by adding new noun features F'_{noun} from the teacher and removing their nearest neighbors, maintaining constant memory size. We then apply K-means clustering to $\mathbf{F}_{\text{mem}}^j$ to obtain K cluster centers $\mathbf{F}_{\text{c}}^j = \{F_{c_1}^j, F_{c_2}^j, \dots, F_{c_K}^j\}$.

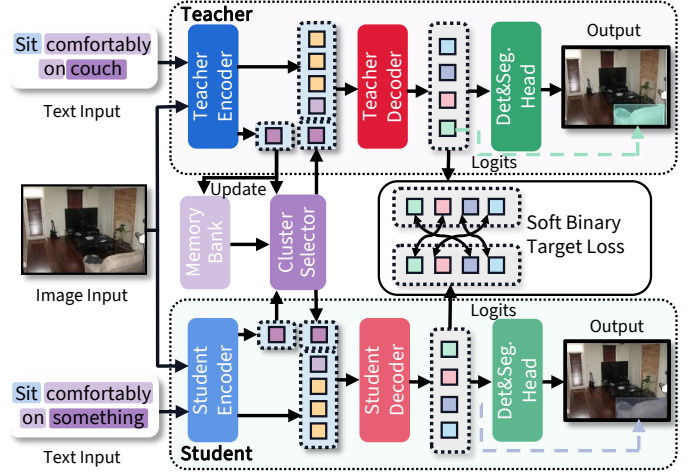


Fig. 5: **Noun-pronoun distillation framework.** Our framework employs parallel teacher-student encoder-decoder architectures for affordance learning. The teacher processes specific noun-based descriptions (e.g., “sit comfortably on couch”), while the student handles generalized pronoun-based inputs (e.g., “sit comfortably on something”). Knowledge transfer occurs through two mechanisms: (i) a memory bank storing noun features that guides the student’s cluster selector, and (ii) a soft binary target loss that aligns teacher-student logits. This design enables category-agnostic inference while maintaining category-informed understanding.

Knowledge transfer occurs through a cluster selector in the student model, which uses nearest neighbor classification to select a prototype $F_{c_s}^j$ from \mathbf{F}_{c}^j based on the pronoun feature F'_{pron} . This prototype replaces F'_{pron} in the student’s feature sequence. To ensure proper alignment, we define the cluster loss $\mathcal{L}_{\text{cluster}} = \|F'_{\text{pron}} - F_{c_s}^j\|_2$, which minimizes the Euclidean distance between the pronoun feature and selected cluster center.

Preference Distillation: We align teacher and student predictions through a soft binary target loss based on the Kullback-Leibler (KL) divergence. For each object query, we compute binary probabilities indicating positive (ground truth object) or negative matches: $\mathbf{p} = [p^{\text{pos}}, p^{\text{neg}}] \in \mathbb{R}^{1 \times 2}$. These probabilities are defined using the softmax function:

$$p^{\text{pos}} = \frac{\sum_{j=1}^{n_{\text{max}}-1} \exp(\hat{g}_j)}{\sum_{j=1}^{n_{\text{max}}} \exp(\hat{g}_j)}, \quad p^{\text{neg}} = \frac{\exp(\hat{g}_{n_{\text{max}}})}{\sum_{j=1}^{n_{\text{max}}} \exp(\hat{g}_j)}, \quad (4)$$

The probability sequences for teacher and student models, denoted as $\mathbf{P}_t = [\mathbf{p}_{t_1}, \dots, \mathbf{p}_{t_{n_{\text{pred}}}}]$ and $\mathbf{P}_s = [\mathbf{p}_{s_1}, \dots, \mathbf{p}_{s_{n_{\text{pred}}}}]$, are aligned through bipartite matching. Using the Hungarian algorithm [75], we find an optimal permutation $\sigma \in \mathfrak{S}_{n_{\text{pred}}}$ that minimizes the matching cost:

$$\hat{\sigma} = \arg \min_{\sigma \in \mathfrak{S}_{n_{\text{pred}}}} \sum_{i=1}^{n_{\text{pred}}} \mathcal{L}_{\text{match}}(y_{t_i}, y_{s_{\sigma(i)}}), \quad (5)$$

where $y_{t_i} = (\hat{b}_{t_i}, \mathbf{p}_{t_i})$ combines the teacher’s bounding box prediction \hat{b}_{t_i} and probabilities, and $\mathcal{L}_{\text{match}}$ incorporates both box prediction losses and KL divergence.

The soft binary target loss is then defined using the optimal assignment $\hat{\sigma}$:

$$\mathcal{L}_{\text{binary}} = \sum_{i=1}^{n_{\text{pred}}} \mathcal{L}_{\text{KL}}(\mathbf{p}_{t_i}, \mathbf{p}_{s_{\hat{\sigma}(i)}}), \quad (6)$$

where the KL divergence between teacher and student proba-

bilities is:

$$\mathcal{L}_{\text{KL}}(\mathbf{p}_{t_i}, \mathbf{p}_{s_{\hat{\sigma}(i)}}) = p_{t_i}^{\text{pos}} \log\left(\frac{p_{t_i}^{\text{pos}}}{p_{s_{\hat{\sigma}(i)}}^{\text{pos}}}\right) + p_{t_i}^{\text{neg}} \log\left(\frac{p_{t_i}^{\text{neg}}}{p_{s_{\hat{\sigma}(i)}}^{\text{neg}}}\right). \quad (7)$$

Minimizing $\mathcal{L}_{\text{binary}}$ aligns the student’s binary query probabilities with the teacher’s. Since the preference score \hat{s}_i (Eq. (2)) follows a similar formulation to p^{pos} , this effectively transfers preference knowledge from teacher to student.

Overall Training Loss: We combine all components into a final training objective for the Afford-X with noun-pronoun distillation:

$$\mathcal{L}_{\text{Afford-X-NP}} = \mathcal{L}_{\text{Afford-X}}^t + \mathcal{L}_{\text{Afford-X}}^s + \lambda_7 \mathcal{L}_{\text{cluster}}^s + \lambda_8 \mathcal{L}_{\text{binary}}^s, \quad (8)$$

where $\mathcal{L}_{\text{Afford-X}}^t$ and $\mathcal{L}_{\text{Afford-X}}^s$ represent the teacher and student model losses, and λ_7, λ_8 weight the distillation components. The distillation losses $\mathcal{L}_{\text{cluster}}^s$ and $\mathcal{L}_{\text{binary}}^s$ apply only to the student model. During inference, we employ only the student model with the fixed memory bank, maintaining category-agnostic object identification.

We provide additional methodological details, including *noun feature* representations in Appx. A and *loss function* derivations in Appx. B. The effectiveness of our proposed modules is validated through extensive experiments detailed in Sec. VI-C and Appx. D. Furthermore, in Sec. VI-B, we demonstrate that the integration of these modules achieves state-of-the-art performance across multiple benchmarks.

D. Verb Attention module and Bi-Fusion module

To enhance multimodal understanding, we introduce two specialized components: the BF module for cross-modal feature integration and the VA module for action-focused reasoning.

BF module: We design this module to overcome limitations of MDETR’s feature concatenation approach by implementing bi-directional cross-modal attention between visual and textual features. This direct interaction captures fine-grained vision-language associations through parallel bi-directional attention:

$$\begin{aligned} F'_v &= F_v + \gamma_v \cdot \text{Attn}_{v \rightarrow t}(\text{LN}(F_v), \text{LN}(F_t)), \\ F'_t &= F_t + \gamma_t \cdot \text{Attn}_{t \rightarrow v}(\text{LN}(F_t), \text{LN}(F_v)), \end{aligned} \quad (9)$$

where $\text{Attn}_{v \rightarrow t}$ and $\text{Attn}_{t \rightarrow v}$ implement multi-head attention between modalities, LN performs layer normalization, and learnable parameters γ_v, γ_t control cross-modal influence.

VA module: This module enhances action-related information processing while reducing interference from dominant object categories. Leveraging the standardized verb-object-preposition format of task descriptions, it applies cross-attention between verb features and the complete textual prompt. Given the first verb’s feature $F_{vb} \in \mathbb{R}^{C_t}$ and full text features $F_t \in \mathbb{R}^{L \times C_t}$ from the text encoder (where L is sequence length and C_t is feature dimension), the module computes:

$$F''_t = F_t + \text{CrossAttn}(\text{LN}(F_t), \text{LN}(F_{vb})), \quad (10)$$

where CrossAttn performs cross-attention to produce enhanced text features F''_t with dimensions matching F_t , effectively amplifying action-related information in the final representation.

E. Summary

The combination of noun-pronoun distillation, bi-directional feature fusion, and verb-focused attention enables Afford-X to effectively reason about object affordances without relying on explicit category labels. The teacher-student framework transfers object-centric knowledge while maintaining category-agnostic inference, the BF module ensures comprehensive multimodal understanding, and the VA module emphasizes action-specific features critical for affordance reasoning. Together, these components form a robust architecture that bridges the gap between category-specific training and category-agnostic deployment while maintaining high performance in affordance detection tasks.

IV. DATASET CONSTRUCTION

We present a scalable approach for creating large-scale affordance knowledge bases through automated conversion of object detection datasets. Our pipeline transforms standard detection annotations into rich affordance-task pairs, yielding two comprehensive datasets: COCO-Aff from COCO and LVIS-Aff from LVIS. We detail our conversion methodology in Sec. IV-A and analyze dataset characteristics in Sec. IV-B.

A. Dataset Collection

A primary challenge in developing Afford-X is establishing comprehensive affordance knowledge without depending on LLM inference. While manual dataset construction is possible, it becomes impractical due to the complex many-to-many relationships between tasks and objects: single objects can serve multiple purposes, tasks can utilize various objects, and objects have different levels of suitability for each task. This intricate mapping makes manual knowledge base construction both time-intensive and potentially inconsistent.

We address this challenge through an automated pipeline that leverages LLM capabilities for dataset construction. Our approach prioritizes three critical factors: task diversity (enabling broad affordance reasoning), image quantity (supporting physical property learning and scene generalization), and object category variety (covering diverse usage scenarios). While existing detection datasets provide rich visual and categorical resources, we needed a systematic method to generate diverse tasks and establish meaningful task-object relationships.

Our pipeline (illustrated in Fig. 6) employs GPT-4 for both task-object pair generation and quality inspection. After filtering uncommon object categories (e.g., animals, musical instruments, food items) that rarely serve as tools, we proceed through four systematic steps:

Step 1: Task Prompt Collection. A GPT-4-based task producer generates 10 diverse tasks per object category, building an initial task pool. This step captures various potential uses for each object, ensuring comprehensive affordance coverage while maintaining natural and practical tasks.

Step 2: Task and Object Category Matching. A GPT-4-based pair producer matches tasks with relevant object categories, incorporating commonsense preference rankings. For instance, in “*drink water with,*” cups receive higher

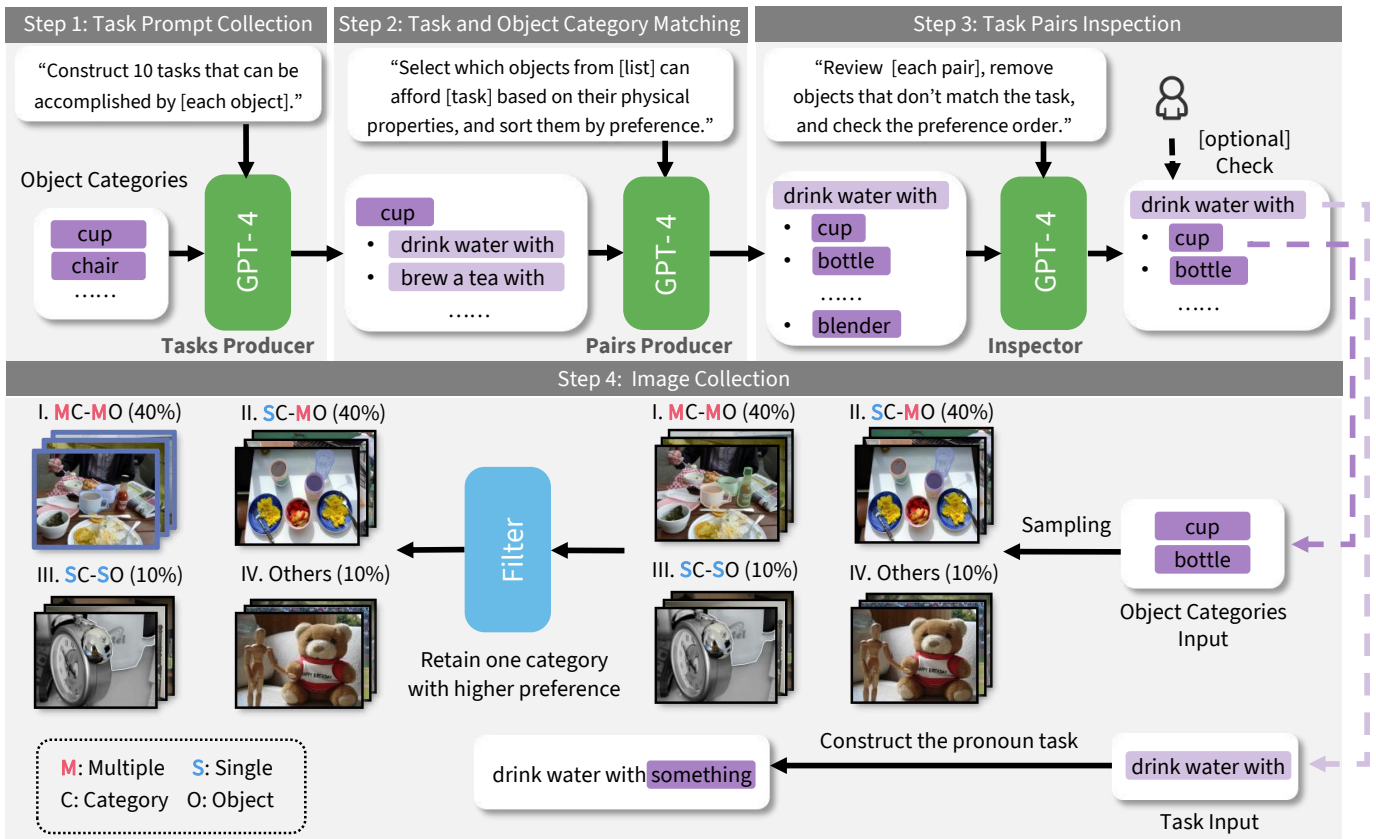


Fig. 6: **Pipeline for affordance dataset construction.** Our automated pipeline transforms detection datasets into affordance knowledge bases through four steps: (i) task generation—creating diverse tasks per object category, (ii) pair matching—associating tasks with suitable objects and establishing affordance rankings, (iii) quality inspection—validating task-object pairs and ranking accuracy, and (iv) image sampling—following composition rules (40% MCMO, 40% SCMO, 10% SCSO, 10% no targets) while retaining highest-priority objects per task. This systematic approach ensures comprehensive coverage of affordance relationships while maintaining data quality.

rankings than bottles, reflecting intuitive usage preferences. This ranking system captures nuanced distinctions in object suitability for specific tasks.

Step 3: Task Pairs Inspection. A GPT-4-based inspector performs multi-level quality control: filtering tasks against predefined criteria, verifying object-task match rankings, and removing inappropriate pairs (e.g., excluding blenders from “drink water with”). An optional manual review reduces task redundancy to optimize training efficiency, though this primarily serves computational rather than quality purposes.

Step 4: Image Collection. Following COCO-Tasks [37], we organize images into four configurations: MCMO (multiple categories, multiple objects), SCMO (single category, multiple objects), SCSO (single category, single object), and Others (random images without target categories). We retain highest-priority objects per task and append “something” to prompts, balancing task specificity with visual diversity.

This automated pipeline enables efficient construction of large-scale affordance datasets while maintaining data quality. By leveraging LLM capabilities for generation and inspection, we create comprehensive knowledge bases that capture complex task-object relationships.

B. Dataset Statistics

Our construction pipeline produced two comprehensive affordance datasets: COCO-Aff and LVIS-Aff. COCO-Aff,

derived from COCO2014 [35], contains 112k images spanning 1130 task prompts and 80 object categories. We partitioned the dataset into training (600 images/task) and test (150 images/task) sets, sampling from COCO2014’s training and validation sets respectively for fair evaluation.

LVIS-Aff represents a significant expansion using LVIS [36], encompassing 119k images, 1494 task prompts, and 1064 object categories. We followed the same sampling strategy, drawing training (600 images/task) and test (150 images/task) sets from COCO2017’s training and validation sets respectively, maintaining strict separation for reliable evaluation.

Both datasets exhibit long-tail distributions in task-object relationships, reflecting natural variations in object functionality. Objects with limited functional diversity generated fewer unique tasks during Step 1 due to task overlap, leading to subsequent filtering. Despite this natural skew, the datasets provide comprehensive coverage of daily-life affordance scenarios, establishing robust knowledge bases for affordance reasoning. More details for the specifications and characteristics of both constructed datasets is presented in Appx. I

V. EMBODIED AFFORDANCE REASONING

We demonstrate Afford-X’s practical applications by integrating it into embodied agents within simulated environments.

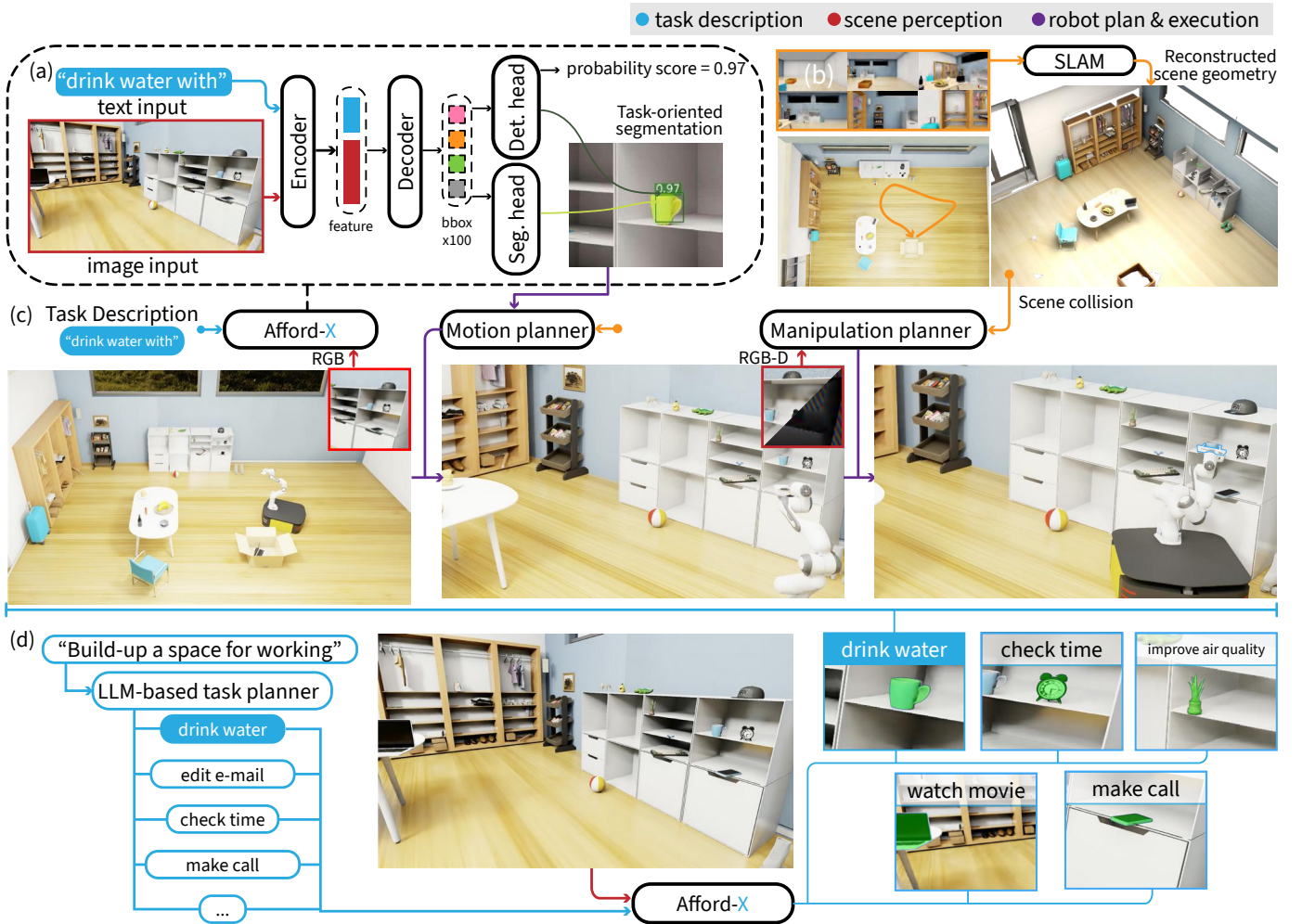


Fig. 7: **System infrastructure for task-oriented manipulation.** Our robot executes the task “drink water with” through a multi-stage process: (a) Afford-X performs initial affordance reasoning on RGB input, generating instance segmentation masks for suitable objects. (b) Optionally, the robot navigates the scene to reconstruct geometric information with SLAM, which is used for planning collision-free motion in completely unseen scenes. (c) The robot executes task-oriented manipulation by selecting an object via Afford-X, approaching for detailed perception, and performing manipulation. (d) For complex tasks (e.g., “build up a space for working”), the system decomposes the high-level goal into sequential sub-tasks, applying procedure (c) to each. Additional examples are provided in Appx. G

Our evaluation examines two key capabilities: scene affordance reasoning—analyzing object affordances in complex 3D environments, and task-oriented manipulation—utilizing affordance understanding for autonomous task execution. We leverage photorealistic rendering techniques from NVIDIA Isaac Sim to provide both high-fidelity rendering and precise ground-truth annotations, enabling systematic assessment of how our model bridges perception and action in embodied contexts.

A. Affordance Reasoning in the Scene

We developed a comprehensive evaluation within NVIDIA Isaac Sim to rigorously evaluate Afford-X’s affordance reasoning in 3D environments. This evaluation assesses the model’s understanding of object-task relationships across diverse environmental configurations and viewing conditions.

Our test environments employ a multi-source scene composition approach. We begin with base scenes from the Ev-

ermotion dataset¹ and OmniGibson [42], providing realistic room layouts and furniture arrangements. We augment these with randomly placed textured meshes from Objaverse [41], following two principles: (i) including both task-suitable and unsuitable objects to test discrimination capability, and (ii) randomized object placement for complexity.

We evaluate Afford-X’s ability in selecting proper object for the desired task in the simulated 3D scenes, and compare it with LLM-integrated pipelines. The evaluation features an RGB-D camera for environmental perception. Isaac Sim’s physics engine ensures authentic environmental interactions, while its ray-tracing renderer generates photorealistic images with lighting and materials. The simulator provides ground-truth annotations including object bounding boxes and segmentation masks for quantitative evaluation. During testing, Afford-X processes RGB images alongside task instructions, generating segmentation masks and for identifying task-relevant objects. This enables the robot to identify

¹<https://evermotion.org/>

suitable objects for task execution. These procedures enables systematic evaluation across varying scenes, viewpoints, and task contexts while maintaining experimental reproducibility.

The results are reported and analyzed in Sec. VI-E. Further towards the open-ended world, Appx. G reports a more in-depth experiments that evaluates Afford-X’s capabilities in diverse 3D scenes.

B. Task-oriented Manipulation

Traditional task-oriented robotics often relies on human supervision or predefined rules for object selection, limiting autonomy in open-world scenarios (as discussed in Sec. II-C). By integrating Afford-X, we enable robots to autonomously identify and interact with task-appropriate objects through affordance-based reasoning.

Our system architecture (Fig. 7) combines affordance understanding with established manipulation frameworks. We employ NVIDIA cuRobo [81] as the motion planner, which utilizes either SLAM-reconstructed or ground-truth scene meshes for collision-aware trajectory generation. Following Ikeuchi’s task-oriented paradigm [64], each task requires either a specialized manipulation module or a general-purpose control strategy. We demonstrate this framework through the typical grasping tasks, where GraspNet [82] serves as the manipulation planner that computes grasp poses using RGB-D input and Afford-X’s segmentation masks.

The manipulation procedure consists of three phases: (i) Affordance perception: Afford-X processes the scene’s RGB frame with a task description, identifying suitable target objects through segmentation masks; (ii) Viewpoint optimization: The robot positions itself at a prescribed viewing distance d_{view} from the identified target for detailed perception, where the target camera location is computed using the depth image additionally acquired in step (i); (iii) Task execution: The manipulation planner generates the target manipulation strategy (grasping pose) and the robot is controlled to execute appropriate manipulation motion. Sec. VI-F demonstrates simulated robot execution in diverse interior scenes for collecting object for diverse tasks.

For complex tasks requiring multiple steps (e.g., “build up a space for working”, Fig. 7(d)), we employ an LLM to decompose the high-level goal into atomic sub-tasks. Each sub-task follows the same three-phase protocol sequentially, enabling structured completion of complex manipulations through affordance-guided action sequences. This integration of affordance reasoning with manipulation planning advances autonomous task-oriented robotics, enabling robots to independently identify and utilize appropriate objects based on task requirements. Appx. H provides more details and qualitative results.

VI. EXPERIMENT

To validate the effectiveness of Afford-X, we conduct comprehensive experiments across three key dimensions: (i) performance comparison and ablation studies (Secs. VI-B and VI-C), (ii) dataset analysis (Sec. VI-D), and (iii) real-world applicability (Secs. VI-E and VI-F). The latter includes

comparative analysis against LLM-based approaches and validation in task-oriented manipulation scenarios.

A. Implementation Details

Model Architecture: We implement Afford-X using RoBERTa-base [83] for text encoding and ResNet-101 [84] as the CNN backbone. To leverage existing vision-language understanding capabilities, we initialize our model with pre-trained weights from MDETR [4]. We evaluate this architecture across three progressively more challenging datasets: COCO-Tasks, COCO-Aff, and LVIS-Aff.

Training Protocol: Our training follows a carefully designed multi-stage approach. In the initial verb-pronoun and verb-noun stages, we employ the Adam optimizer with a batch size of 36, applying a uniform learning rate of 10^{-5} across the text encoder, backbone network, and BF module. The subsequent distillation stage requires more precise parameter updates, leading us to reduce the batch size to 18 and adjust the text encoder learning rate to 5×10^{-6} while maintaining other learning rates.

Data Augmentation: To enhance model robustness to real-world variations, we implement a comprehensive data augmentation pipeline. This includes dynamic image resizing that randomly scales the shortest side between 480-800 pixels while capping the longest side at 1333 pixels. We further augment the training data through random cropping (probability 0.5), generating diverse viewports between 384-1333 pixels.

Evaluation Metrics: We evaluate model performance using the AP@0.5 metric, which assesses localization accuracy and ranking effectiveness through predicted preference scores S_{pred} . For comprehensive evaluation across different tasks, we report the mean Average Precision (mAP@0.5), calculated by averaging AP@0.5 scores across all experimental tasks.

B. Performance Analysis

Our comprehensive experimental results are presented in Tab. II. We evaluate our approach against existing methods based on pre-trained MMs, excluding LLM-augmented baselines for fair comparison. Prior approaches fall into two categories: two-stage methods combining object detection with Gated Graph Neural Networks (GGNN) [53] (rows (a)-(g)), and one-stage methods built on MDETR (rows (h)-(k)).

In the two-stage category, we evaluated three object detection frameworks combined with GGNN: CNN-based Fast R-CNN [79], YOLO (version 11), and transformer-based approaches (MDETR, ViTDet [80]). Despite using COCO-pretrained weights, these methods showed limited performance. Even on the relatively simple COCO-Tasks dataset, Fast R-CNN and YOLO implementations achieved only 32-33% mAP^{box}. While ViTDet offered modest improvements, scaling from ViT-B to ViT-H backbone failed to overcome fundamental performance limitations.

The one-stage category, represented by MDETR-based approaches, demonstrated notably stronger results. The baseline MDETR implementation (row (h)) achieved 41.3% mAP^{box} and 35.2% mAP^{mask} on COCO-Tasks, suggesting that vision-language aligned features better capture object semantics

TABLE II: **Comparison of Afford-X with state-of-the-art methods.** Comprehensive evaluation across COCO-Tasks, COCO-Aff, and LVIS-Aff datasets demonstrates the effectiveness of our approach, with Afford-X consistently achieving superior performance in both affordance understanding and instance segmentation tasks. The performance gains stem from our proposed VA and BF modules, which enhance the baseline architecture. Results marked with † are from original papers, with ‡ are from our previous conference work, and with **bold** and underlined values indicating best and second-best performance, respectively.

Index	Method	COCO-Tasks		COCO-Aff		LVIS-Aff	
		mAP ^{box}	mAP ^{mask}	mAP ^{box}	mAP ^{mask}	mAP ^{box}	mAP ^{mask}
(a)	Fast R-CNN [79] + GGNN [†]	32.6	-	-	-	-	-
(b)	YOLO + GGNN [53] [†]	33.2	-	-	-	-	-
(c)	MDETR (w/o pretraining) + GGNN [‡]	9.6	8.6	-	-	-	-
(d)	MDETR + GGNN [‡]	36.8	30.3	-	-	-	-
(e)	ViTDet (ViT-B) [80] + GGNN	22.5	29.5	27.4	22.8	6.6	5.9
(f)	ViTDet (ViT-L) + GGNN	32.1	24.6	29.7	24.7	8.0	7.1
(g)	ViTDet (ViT-H) + GGNN	33.8	25.9	31.5	26.1	8.5	7.4
(h)	MDETR [4]	41.3 [‡]	35.2 [‡]	44.7	41.0	25.1	22.7
(i)	MDETR (w/ VA & BF)	43.2	36.9	<u>45.2</u>	<u>41.4</u>	<u>26.8</u>	<u>24.2</u>
(j)	TOIST [15]	<u>44.1</u> [‡]	<u>39.0</u> [‡]	44.9	41.3	26.2	23.4
(k)	Afford-X (w/ VA & BF)	45.3	39.2	45.8	42.5	27.7	24.8

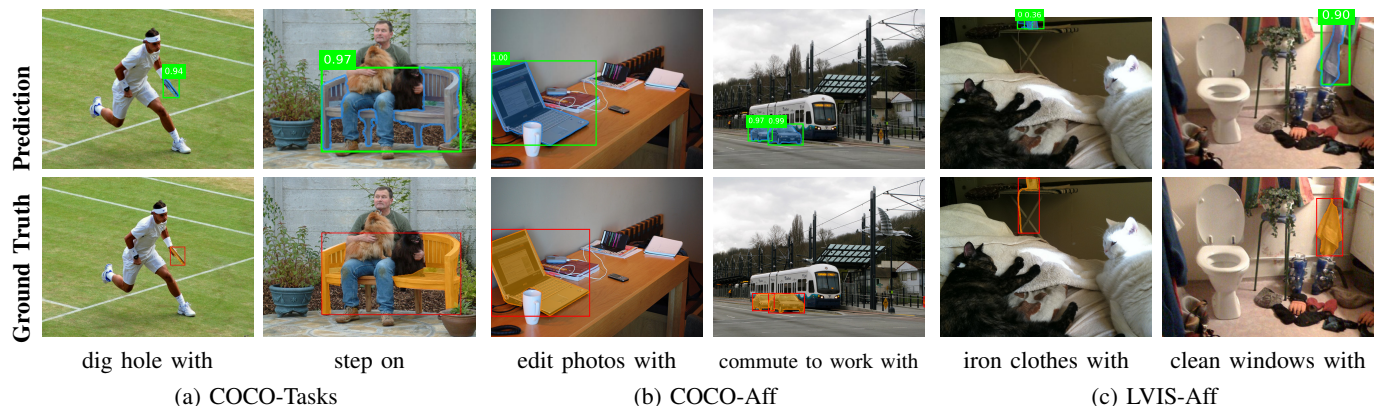


Fig. 8: **Qualitative results of Afford-X on three datasets.** The first row of each section shows model predictions, with corresponding ground truth in the second row. Results demonstrate performance across (a) COCO-Tasks, showing sports and office scenes; (b) COCO-Aff, depicting indoor and outdoor environments; and (c) LVIS-Aff, illustrating diverse interaction scenarios. Green boxes indicate model predictions while orange boxes show ground truth annotations.

across diverse scenarios. Importantly, this one-stage approach significantly outperformed its two-stage counterpart (row (d)), despite sharing the same MDETR detection backbone. This performance gap highlights the advantages of end-to-end training for affordance reasoning tasks.

Building on these insights, we enhanced the baseline MDETR with our proposed VA and BF modules. This enhancement yielded substantial improvements across all datasets: COCO-Tasks performance increased to 43.2% mAP^{box} and 36.9% mAP^{mask}, with similar gains on COCO-Aff and LVIS-Aff. Our full Afford-X framework, which integrates these modules with TOIST, further pushes performance boundaries, achieving 45.3% mAP^{box} and 39.2% mAP^{mask} on COCO-Tasks. Notably, Afford-X maintains its leading position on the more challenging LVIS-Aff dataset, which features long-tail distributions and diverse affordance relationships, reaching 27.7% mAP^{box} and 24.8% mAP^{mask}.

Qualitative results in Fig. 8 reveal both strengths and limitations across all three datasets. While Afford-X successfully identifies major affordance regions, it sometimes struggles with fine-grained functional elements crucial for complete

affordance understanding. For instance, in the “iron clothes with” example, the model misses the iron’s power cord, while the “clean windows with” case shows imprecise bounding box localization extending beyond the cleaning implement.

C. Ablation Study

We conduct comprehensive ablation studies to evaluate three critical components of Afford-X: (i) distillation architecture, (ii) VA and BF modules, and (iii) cluster number K. Using the TOIST framework as our baseline, we systematically analyze each component’s contribution through extensive experiments.

Knowledge Transfer through Distillation: To address categorical bias in the COCO-Tasks dataset, we introduce a novel two-stage Noun-Pronoun Distillation framework. Rather than directly minimizing the distance between pronoun-based ($l_{\text{pron}}^{\text{tr}}$) and noun-based ($l_{\text{noun}}^{\text{tr}}$) representations, our framework strategically transfers knowledge through an intermediate feature space ($l_{c_s}^j$). This is achieved by first training a teacher model with explicit noun categories and then distilling this knowledge into a baseline model operating on verb-pronoun instructions. As shown in Tab. III, this approach improves

the verb-pronoun mAP^{box} from 43.4% to 44.1% compared to a plain trained MDETR. Notably, this sophisticated distillation strategy outperforms direct distillation between $l_{\text{pron}}^{\text{tr}}$ and $l_{\text{noun}}^{\text{tr}}$, confirming the effectiveness of our architectural design.

TABLE III: **Different distillation methods on COCO-Tasks.** Values in parentheses show improvements over the baseline.

Method	mAP^{box}	mAP^{mask}
MDETR	41.3	35.2
distill from $l_{c_2}^j$ to $l_{\text{pron}}^{\text{tr}}$	44.1 (+2.8)	39.0 (+3.8)
distill from $l_{\text{noun}}^{\text{tr}}$ to $l_{\text{pron}}^{\text{tr}}$	41.9 (+0.6)	36.0 (+0.8)

To further refine feature grouping and preference scoring, we propose a Clustering Distillation (CD) approach comprising three complementary components: Cluster Center Replacement (CCR) for anchoring pronoun tokens, Cluster Loss (CL) to promote refined feature grouping, and Soft Binary Target Loss (SBTL) to improve preference modeling. As demonstrated in Tab. IV, while individual components provide modest improvements, their combination yields substantial gains of +2.8% mAP^{box} and +3.8% mAP^{mask} over the baseline. When integrated into the complete Afford-X framework, these enhancements achieve state-of-the-art performance of 45.3% mAP^{box} on verb-pronoun tasks.

TABLE IV: **Ablation study of clustering distillation components on COCO-Tasks.** Each row shows performance impact when specific components are enabled (\checkmark) or disabled (\times). CCR: Cluster Center Replacement, CL: Cluster Loss, SBTL: Soft Binary Target Loss.

Index	Method Components			Performance	
	CCR	CL	SBTL	mAP^{box}	mAP^{mask}
(a)	\times	\times	\times	41.3	35.2
(b)	\times	\times	\checkmark	43.4 (+2.1)	38.0 (+2.8)
(c)	\times	\checkmark	\times	42.0 (+0.7)	37.1 (+1.9)
(d)	\times	\checkmark	\checkmark	43.8 (+2.5)	38.6 (+3.4)
(e)	\checkmark	\times	\times	42.0 (+0.7)	37.0 (+1.8)
(f)	\checkmark	\times	\checkmark	42.3 (+1.0)	37.3 (+2.1)
(g)	\checkmark	\checkmark	\times	42.3 (+1.0)	37.5 (+2.3)
(h)	\checkmark	\checkmark	\checkmark	44.1 (+2.8)	39.0 (+3.8)

Analysis of VA and BF Modules: Tab. V presents ablation results for the VA and BF modules across three input settings: verb-pronoun, verb-noun, and distill. We evaluate their effectiveness by sequentially integrating these modules into our baseline model.

TABLE V: **Ablation study of Afford-X components.** Analysis showing performance impact of VA and BF modules across verb-pronoun, verb-noun, and distillation settings. Values in parentheses indicate improvements over baseline configuration.

Index	Method		Performance		
	VA	BF	verb-pronoun	verb-noun	distill
(a)	\times	\times	41.3	53.2	44.1
(b)	\checkmark	\times	43.2 (+1.9)	53.8 (+0.6)	44.8 (+0.7)
(c)	\times	\checkmark	43.0 (+1.7)	53.9 (+0.7)	44.6 (+0.5)
(d)	\checkmark	\checkmark	43.4 (+2.1)	54.8 (+1.6)	45.3 (+1.2)

Individual module integration shows consistent improvements across all input configurations. The VA module (row (b)) yields gains of +1.9%, +0.6%, and +0.7% across the three

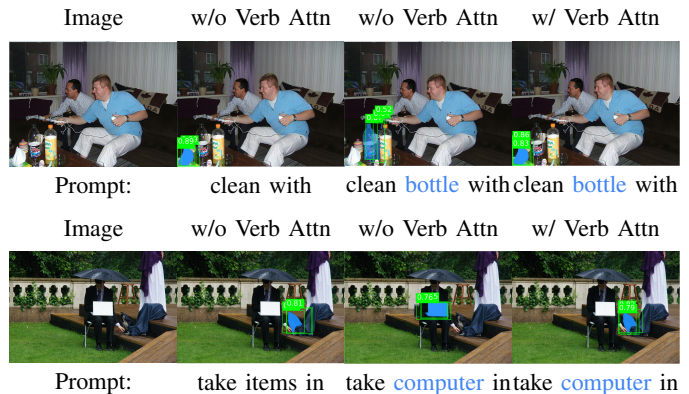


Fig. 9: **Impact of VA module on affordance reasoning performance.** The VA module reduces failures in affordance reasoning when text prompts include prominent objects. Column 1 shows the original images. Columns 2 and 3 present results without the module for prompts without and with object labels, respectively. Column 4 displays results with the module for prompts with object labels.

input types, demonstrating its effectiveness in emphasizing action-related cues while reducing noun-based interference. Similarly, the BF module (row (c)) improves performance by +1.7% and +0.7% for pretrained student and teacher models respectively, with an additional +0.5% gain during distillation, confirming that bidirectional cross-modal attention enhances visual-language alignment for affordance reasoning.

The combination of both modules (row (d)) demonstrates synergistic benefits, achieving +2.1% improvement for verb-pronoun input and +1.6% for verb-noun input, surpassing individual module gains. While the joint implementation shows a more modest +1.2% improvement under the distill setting, likely due to architectural constraints, these results validate the complementary nature of both modules in enhancing affordance reasoning.

Qualitative analysis in Fig. 9 illustrates the VA module’s impact on attention mechanisms. The baseline model correctly identifies target objects for tasks like “clean with” (towel) and “take item in” (backpack) but becomes susceptible to interference from distracting nouns (bottle and computer). With the VA module, the model maintains accurate affordance reasoning while effectively filtering such distractions, providing visual confirmation of our quantitative findings and demonstrating enhanced functional reasoning capabilities. Additional visualization results can be found in Appendix B.

Analysis of Cluster Number K: We systematically investigate optimal cluster numbers (K) in the distillation framework; see also Fig. 10. We evaluate K values from 1 to 10, noting that higher values introduce excessive clustering complexity. Results show that all tested configurations improve upon the baseline model’s performance (41.3% mAP^{box} , 35.2% mAP^{mask}). $K = 3$ emerges as the optimal choice, suggesting that a moderate number of clusters effectively balances feature aggregation and information preservation during knowledge distillation from noun features to the student model.

D. Dataset Analysis

To examine how large-scale visual and linguistic information improves affordance reasoning, we analyze two key

factors: *task-scale* and *category-scale*.

Task-scale Analysis: We evaluate models trained on three datasets of increasing scale: COCO-Tasks (14 tasks), COCO-Aff (1,144 tasks), and LVIS-Aff (1,496 tasks). As shown in Tab. VI, while the COCO-Tasks-trained model achieves strong performance on seen tasks ($mAP^{\text{box}} = 45.3\%$), it fails to generalize to unseen tasks ($mAP^{\text{box}} = 1.6\%$). In contrast, training on COCO-Aff substantially improves generalization to unseen tasks ($mAP^{\text{box}} = 24.5\%$), with further gains achieved by LVIS-Aff ($mAP^{\text{box}} = 26.3\%$), demonstrating the benefits of expanded task and object coverage.

TABLE VI: **Task-scale analysis.** Comparison of model performance on 14 *seen tasks* from COCO-Tasks and 80 *unseen tasks* from LVIS.

Training Data.	Seen-Tasks (14)		Unseen-Tasks (80)	
	mAP^{box}	mAP^{mask}	mAP^{box}	mAP^{mask}
COCO-Tasks	45.3	39.2	1.6	1.3
COCO-Aff	43.9	38.3	24.5	24.1
LVIS-Aff	—	—	26.3	25.6

Category-scale Analysis: We further evaluate generalization using 40 unseen tasks: 20 with common categories (present in both COCO and LVIS) and 20 with novel categories (LVIS-exclusive). As shown in Tab. VII, the COCO-Aff-trained model performs well on common category tasks (35.0% mAP^{box}) but struggles with novel categories (4.9% mAP^{box}). Models trained on LVIS-Aff show improved performance across both task types (37.2% and 8.3% mAP^{box} respectively), demonstrating that expanded category coverage enhances both affordance reasoning and generalization.

TABLE VII: **Category-scale analysis.** Performance comparison between COCO-Aff and LVIS-Aff trained models on unseen tasks involving common categories (shared between COCO/LVIS) and novel categories (LVIS-exclusive).

Training Data.	Common categories		Novel categories	
	mAP^{box}	mAP^{mask}	mAP^{box}	mAP^{mask}
COCO-Aff	35.0	33.9	4.9	4.8
LVIS-Aff	37.2	35.3	8.3	8.2

E. Affordance Reasoning in 3D Scenes

We evaluate Afford-X’s potential as an alternative to LLMs in robotic deployments through extensive testing in simulated

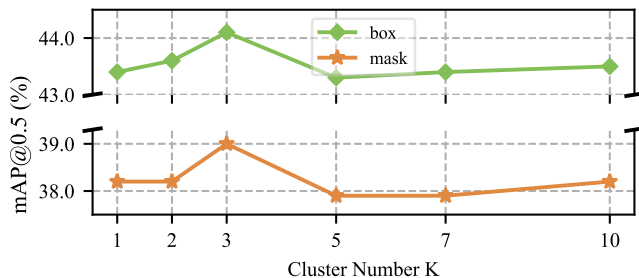


Fig. 10: **Effects of clustering number.** We study the influence of Self-Attention (SA) layers and clustering number on our baseline model. The curves reveal the influence of cluster number selection in the distillation process.

3D environments with textured object meshes, as described in Sec. V-A. Our evaluation compares baseline methods trained on COCO-Aff and LVIS-Aff against three categories of LLM-based pipelines: (i) Detect before Reasoning (row (a) and (b)), where object detection precedes LLM processing; (ii) Reason before Detection (rows (c)-(e)), where LLM identifies candidate objects before guided detection; and (iii) Simultaneous Perception and Reasoning (rows (f)-(h)), where the model jointly processes task and image for direct bounding box output.

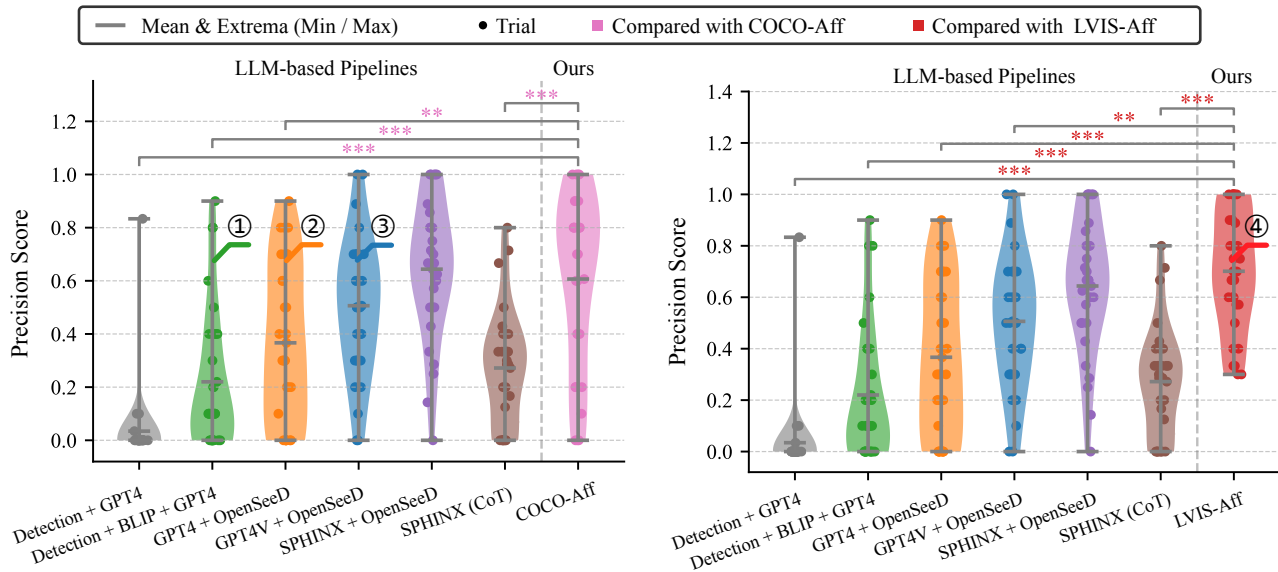
Our experimental framework encompasses 50 tasks (30 seen, 20 unseen) in simulated environments, with each task evaluated across 10 images containing three candidate objects—one capable of affording the task and two non-affording objects randomly selected from the candidate pool. Success criteria require bounding box predictions to achieve mIoU above 0.5, as shown in Fig. 11, where the “Detection” methods utilize RAM++ [85] and Grounding Dino [8] for object detection based on given labels. To ensure practical relevance, all evaluations were conducted on a single 24GB RTX 3090 GPU, comparing API-based services with memory-constrained ($\leq 24\text{GB}$) SPHINX tiny models while accounting for API communication latency in GPT-4 implementations. The FPS and parameter sizes for each baseline are detailed in Tab. VIII, where $>$ indicates API usage, excluding these model parameters from statistics.

TABLE VIII: **Computational efficiency comparison.** Analysis of FPS and the number of parameters across LLM-based pipelines and our proposed approaches, measured on the standard NVIDIA 3090 GPU workstation.

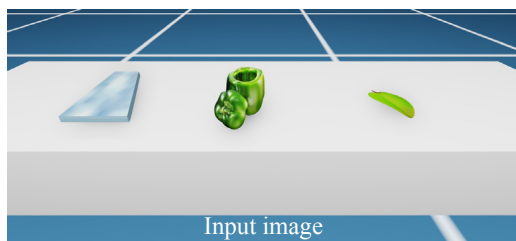
Index	Method	FPS	Parameters
(a)	Detection + GPT-4	1.18	$>369\text{M}$
(b)	Detection + BLIP [40] + GPT-4	0.27	$>498\text{M}$
(c)	GPT-4 + OpenSeeD [86]	0.11	$>116\text{M}$
(d)	GPT-4V + OpenSeeD	0.04	$>116\text{M}$
(e)	SPHINX [26] + OpenSeeD	0.11	1.2B
(f)	SPHINX (CoT)	0.49	1.1B
(g)	COCO-Aff	2.38	187M
(h)	LVIS-Aff	2.38	187M

The experimental results revealed significant performance variations across pipeline architectures. LLM-based label reasoning pipelines demonstrated notably poor performance (2.33% recall, 3.44% mAP), primarily due to semantic ambiguity in object labeling—exemplified by cases where distinct tools like hammers and chisels share generic labels, compromising reasoning accuracy. While image captioning integration showed improvements, limited caption semantic density continued to impede accurate object identification.

Approaches employing initial LLM label generation followed by detection showed improved results, with GPT-4V achieving 49.61% recall and 50.63% mAP. However, this performance remained slightly below the SPHINX model, potentially due to GPT-4V’s inherent value-based constraints on safety and societal norms, particularly evident in scenarios like “hold water” tasks where unconventional but viable solutions like bamboo tubes might be overlooked. End-to-end MLLM systems, while promising, faced practical limitations—the



(a) Precision comparison of different methods



Task: drink water with

- ① Textual ambiguity
- ⊗ "glass, green pepper, leaf"
 - ⊗ "glass"
- ② Missing Perception
- ⊗ "water bottle, glass, mug, straw, water dispenser, sports sipper"
 - ⊗ Detection failed



(b) Analysis of method performance in affordance reasoning

Fig. 11: Comparison between Afford-X and LLM-based methods. Afford-X demonstrates superior performance in affordance reasoning through two key analyses. First, quantitative precision comparisons reveal significant advantages over LLM-based methods, as shown in (a) the violin plot where statistical significance is denoted by stars. Second, (b) qualitative analysis highlights Afford-X's ability to overcome two fundamental limitations of LLM-based approaches: textual ambiguity and limited perception capabilities. While LLMs struggle with semantic uncertainties and visual interpretation, Afford-X successfully identifies and selects objects based on their functional affordances.

memory-constrained SPHINX tiny model required supplementary detection algorithms or chain of thought methods for bounding box output, achieving 39.76% mAP at 0.49 FPS,

indicating limited practical utility.

In contrast, Afford-X demonstrated superior performance through direct bounding box output, achieving 60.67% mAP

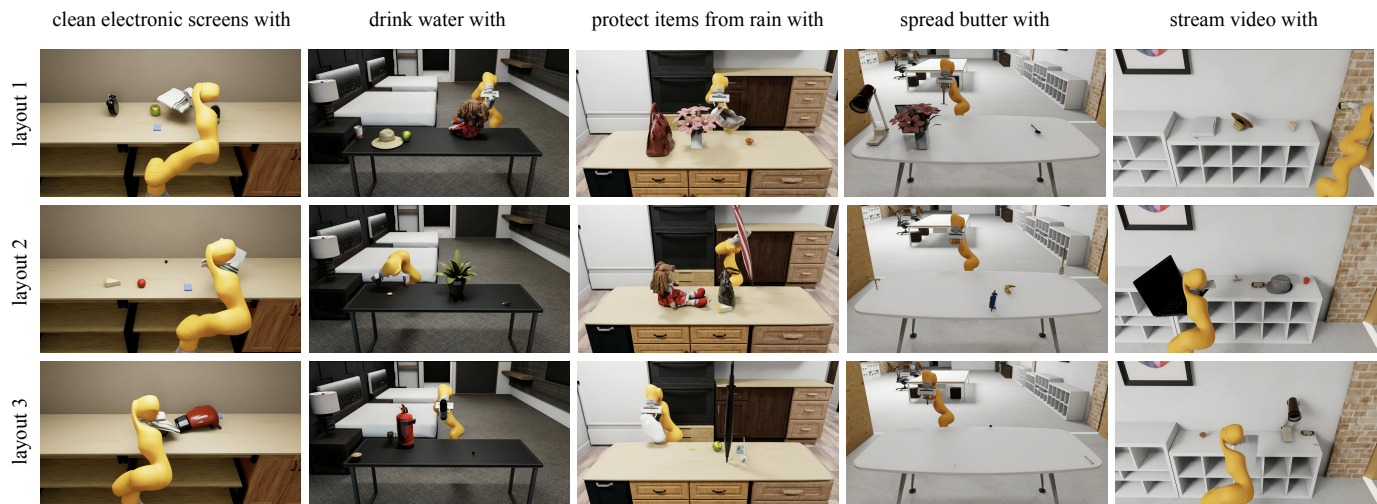


Fig. 12: Task-oriented manipulation across different layouts in simulated environments. The robotic system integrated with Afford-X demonstrates versatile task-oriented manipulation capabilities across various spatial and object configurations in simulated environments, successfully completing multiple affordance-based tasks.

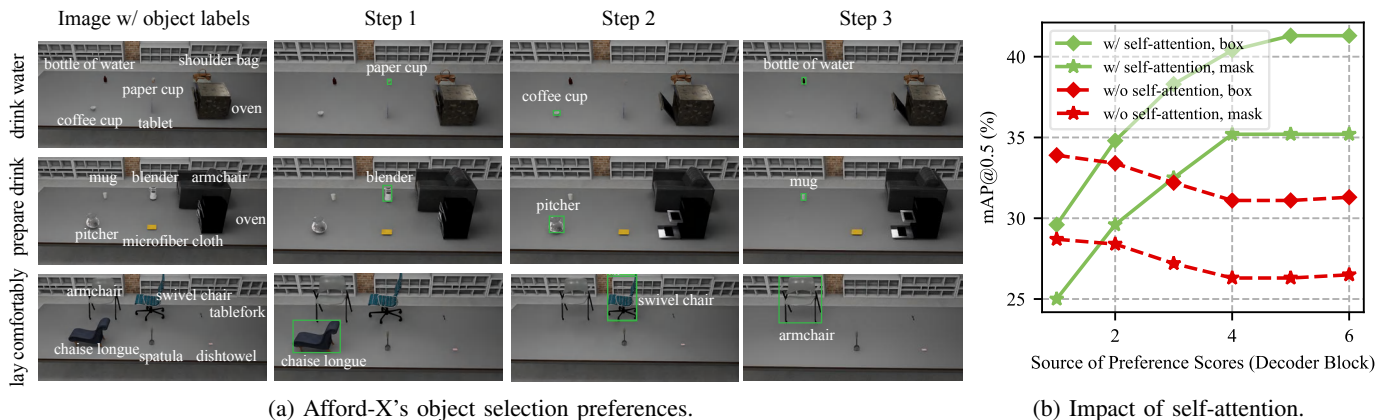


Fig. 13: **Sequential object preference and self-attention analysis.** (a) We demonstrate Afford-X’s affordance-based selection process across three sequential steps. The model exhibits hierarchical preferences as objects are progressively removed from the environment. Each experimental row presents a different task scenario where available objects are labeled to show possible choices. (b) The performance curves reveal the significant impact of self-attention layers on preference modeling. Our analysis shows that models with self-attention consistently achieve higher accuracy across decoder blocks compared to variants without this mechanism.

on COCO-Aff and 67.26% mAP on LVIS-Aff while maintaining 2.38 FPS. These results emphasize the importance of specialized task-oriented datasets for training efficient end-to-end models. Qualitative analysis through four representative case studies revealed the limitations of existing approaches—detection models struggled with semantic ambiguity (particularly in “glass” interpretation between structural glass and drinking vessels), while LLMs without visual perception showed a tendency to infer non-existent objects. Both MLLM and our proposed model exhibited advanced affordance understanding, successfully identifying unconventional object affordances, such as recognizing modified green peppers as viable containers.

This comprehensive evaluation demonstrates that domain-specific training can outperform generic pre-trained MLLM models for affordance reasoning tasks, suggesting a promising direction for practical robotic applications.

F. Task-oriented Manipulation in Diverse Environments

To validate our model’s practical applicability and generalization capabilities, we conducted comprehensive evaluations through a series of systematic experiments in simulated environments. These experiments were designed to assess Afford-X’s adaptability in diverse indoor contexts, utilizing controlled virtual environments to ensure precise manipulation of experimental variables, including object placement, scene complexity, and task parameters. For simplicity, we attach the object to the gripper when it is close enough to the gripper. We present representative environments from the Evermotion dataset used in our evaluation in Fig. A5 in the Appendix G.”

Robot Evaluation in Indoor Scenarios: Our primary evaluation focuses on the robot’s performance across distinct indoor settings—dining room, living room, and office—each rendered in multiple stylistic variants with varying object configurations. We tasked the robot with performing affordance-based grasping (e.g., “drink water with”) that align with typical user interactions in residential and workplace settings. Figs. 12 and A5 illustrates the results in a table-top manipulation

setting using a fixed KUKA IIWA-Panda robot arm. The manipulation is performed within various scenes featuring substantial variation in object placement, room layouts, and environmental complexity, providing a comprehensive test of our model’s adaptability.

Further, Appx. H demonstrates long-horizon task-oriented manipulation capabilities under a larger interior scene with more objects in sight. After decomposing the complex task into multiple steps with an LLM-based task planner, a mobile base manipulator grasps and collects the necessary objects identified by Afford-X accordingly.

Preference on Multiple Options: In real-world scenarios where multiple options are available for the same task, Afford-X demonstrates sophisticated preference modeling aligned with human utility patterns. For instance, when prompted with “prepare drinks with,” the model exhibits hierarchical understanding of utility, prioritizing a blender, followed by a pitcher, and finally a mug. To systematically evaluate this capability, we designed an experimental setup featuring six candidate objects placed on a large table in an interior scene, including three positive object categories for specific tasks (e.g., “prepare drinks with” or “lay comfortably on”). Through an iterative elimination procedure, the robot selects the object with the highest score, which is subsequently removed from the environment for the next query. This process, illustrated in Fig. 13a, thoroughly tests the model’s ability to dynamically adapt its preferences. Similarly, for the task “lay comfortably on,” the model demonstrates nuanced understanding by favoring a lounge over a chair, indicating awareness of comfort-oriented furniture hierarchies.

The model’s sophisticated preference modeling capability is fundamentally enabled by self-attention (SA) layers in the decoder. To validate this mechanism, we conducted a comparative analysis between two model variants—one incorporating SA layers and one without—while maintaining identical parameter budgets to isolate the SA component’s contribution. Using bounding boxes and masks generated by the final decoder block, we computed mean Average Precision (mAP) values based on preference scores from each intermediate de-

coder layer. The SA-equipped model demonstrates progressive improvement through deeper decoder layers, achieving final scores of 41.3% (mAP^{box}) and 35.2% (mAP^{mask}) from initial values of 29.6% and 25.0%, respectively. In contrast, the non-SA version shows limited improvement, reaching maximum values of only 33.9% (mAP^{box}) and 28.7% (mAP^{mask}). These results directly implicate SA layers as crucial components in capturing and refining pairwise preferences—a critical capability for strategic decision-making in progressive object selection tasks.

For comprehensive results and detailed analyses beyond the scope of this section, readers are directed to Appx. G.

VII. CONCLUSION

We present Afford-X, a novel framework addressing a fundamental challenge in robotics: achieving sophisticated affordance reasoning while maintaining computational efficiency for local deployment. Our approach integrates a noun-pronoun distillation pipeline with specialized VA and BF modules, complemented by an automated pipeline for constructing comprehensive affordance reasoning datasets—COCO-Aff and LVIS-Aff. Through extensive experimentation, we demonstrate our framework’s enhanced generalization capabilities while maintaining real-time processing speeds, validated through robotic manipulation experiments in simulated environments.

Our current framework faces two primary limitations. First, geometric features alone prove insufficient for certain affordance reasoning scenarios—for instance, distinguishing between drinking cups and toothbrush holders despite identical geometric features, where usage context and hygiene considerations necessitate different affordances. Second, the lack of 3D information constrains system performance in complex spatial environments, particularly in assessing object relationships and occlusion scenarios. Future work could address these limitations through integration of contextual knowledge bases and incorporation of depth information to enhance spatial understanding.

REFERENCES

- [1] J. J. Gibson, “The theory of affordances. the ecological approach to visual perception,” *The people, place and, space reader*, pp. 56–60, 1979.
- [2] Y. Zhu, T. Gao, L. Fan, S. Huang, M. Edmonds, H. Liu, F. Gao, C. Zhang, S. Qi, Y. N. Wu, *et al.*, “Dark, beyond deep: A paradigm shift to cognitive ai with humanlike common sense,” *Engineering*, vol. 6, no. 3, pp. 310–345, 2020.
- [3] D. Marr, *Vision: A computational investigation into the human representation and processing of visual information*. MIT press, 2010.
- [4] A. Kamath, M. Singh, Y. LeCun, G. Synnaeve, I. Misra, and N. Carion, “Mdetr-modulated detection for end-to-end multi-modal understanding,” in *Proceedings of International Conference on Computer Vision (ICCV)*, 2021.
- [5] C. Jia, Y. Yang, Y. Xia, Y.-T. Chen, Z. Parekh, H. Pham, Q. Le, Y.-H. Sung, Z. Li, and T. Duerig, “Scaling up visual and vision-language representation learning with noisy text supervision,” in *Proceedings of International Conference on Machine Learning (ICML)*, 2021.
- [6] A. Radford, J. W. Kim, C. Hallacy, A. Ramesh, G. Goh, S. Agarwal, G. Sastry, A. Askell, P. Mishkin, J. Clark, *et al.*, “Learning transferable visual models from natural language supervision,” in *Proceedings of International Conference on Machine Learning (ICML)*, 2021.
- [7] L. H. Li, P. Zhang, H. Zhang, J. Yang, C. Li, Y. Zhong, L. Wang, L. Yuan, L. Zhang, J.-N. Hwang, *et al.*, “Grounded language-image pre-training,” in *Proceedings of Conference on Computer Vision and Pattern Recognition (CVPR)*, 2022.
- [8] S. Liu, Z. Zeng, T. Ren, F. Li, H. Zhang, J. Yang, C. Li, J. Yang, H. Su, J. Zhu, *et al.*, “Grounding dino: Marrying dino with grounded pre-training for open-set object detection,” *arXiv preprint arXiv:2303.05499*, 2023.
- [9] M. Qin, J. Brawer, and B. Scassellati, “Robot tool use: A survey,” *Frontiers in Robotics and AI*, vol. 9, p. 1009488, 2023.
- [10] R. Wu, K. Cheng, Y. Zhao, C. Ning, G. Zhan, and H. Dong, “Learning environment-aware affordance for 3d articulated object manipulation under occlusions,” in *Proceedings of Advances in Neural Information Processing Systems (NeurIPS)*, 2024.
- [11] K. Vaesen, “The cognitive bases of human tool use,” *Behavioral and Brain Sciences*, vol. 35, no. 4, pp. 203–218, 2012.
- [12] T. McCormack, C. Hoerl, and S. Butterfill, *Tool use and causal cognition*. Oxford University Press, 2011.
- [13] Y. Zhu, Y. Zhao, and S. Chun Zhu, “Understanding tools: Task-oriented object modeling, learning and recognition,” in *Proceedings of Conference on Computer Vision and Pattern Recognition (CVPR)*, 2015.
- [14] M. Hassanin, S. Khan, and M. Tahtali, “Visual affordance and function understanding: A survey,” *ACM Computing Surveys (CSUR)*, vol. 54, no. 3, pp. 1–35, 2021.
- [15] P. Li, B. Tian, Y. Shi, X. Chen, H. Zhao, G. Zhou, and Y.-Q. Zhang, “Toist: Task oriented instance segmentation transformer with noun-pronoun distillation,” in *Proceedings of Advances in Neural Information Processing Systems (NeurIPS)*, 2022.
- [16] J. Tang, G. Zheng, J. Yu, and S. Yang, “Cotdet: Affordance knowledge prompting for task driven object detection,” in *Proceedings of International Conference on Computer Vision (ICCV)*, 2023.
- [17] M. Qu, Y. Wu, W. Liu, X. Liang, J. Song, Y. Zhao, and Y. Wei, “Rio: A benchmark for reasoning intention-oriented objects in open environments,” in *Proceedings of Advances in Neural Information Processing Systems (NeurIPS)*, 2024.
- [18] K. Fang, Y. Zhu, A. Garg, A. Kurenkov, V. Mehta, L. Fei-Fei, and S. Savarese, “Learning task-oriented grasping for tool manipulation from simulated self-supervision,” *International Journal of Robotics Research (IJRR)*, vol. 39, no. 2-3, pp. 202–216, 2020.
- [19] Z. Wang and G. Tian, “Task-oriented robot cognitive manipulation planning using affordance segmentation and logic reasoning,” *IEEE Transactions on Neural Networks and Learning Systems*, 2023.
- [20] Z. Zhang, Z. Jiao, W. Wang, Y. Zhu, S.-C. Zhu, and H. Liu, “Understanding physical effects for effective tool-use,” *IEEE Robotics and Automation Letters (RA-L)*, vol. 7, no. 4, pp. 9469–9476, 2022.
- [21] K. R. Allen, K. A. Smith, and J. B. Tenenbaum, “Rapid trial-and-error learning with simulation supports flexible tool use and physical reasoning,” *Proceedings of the National Academy of Sciences (PNAS)*, vol. 117, no. 47, pp. 29302–29310, 2020.
- [22] J. Suder, K. Podbucki, and T. Marciniak, “Power requirements evaluation of embedded devices for real-time video line detection,” *Energies*, vol. 16, no. 18, p. 6677, 2023.
- [23] J. Achiam, S. Adler, S. Agarwal, L. Ahmad, I. Akkaya, F. L. Aleman, D. Almeida, J. Altenschmidt, S. Altman, S. Anadkat, *et al.*, “Gpt-4 technical report,” *arXiv preprint arXiv:2303.08774*, 2023.
- [24] F. J. R. Lera, C. F. Llamas, Á. M. Guerrero, and V. M. Olivera, “Cybersecurity of robotics and autonomous systems: Privacy and safety,” in *Robotics-legal, ethical and socioeconomic impacts*, InTech London, UK, 2017.
- [25] I. N. Mseer and S. M. Ahmed, “Artificial intelligence and security challenges,” in *From Industry 4.0 to Industry 5.0: Mapping the Transitions*, pp. 49–55, Springer, 2023.
- [26] Z. Lin, D. Liu, R. Zhang, P. Gao, L. Qiu, H. Xiao, H. Qiu, W. Shao, K. Chen, J. Han, S. Huang, Y. Zhang, X. He, Y. Qiao, and H. Li, “Sphinx: A mixer of weights, visual embeddings and image scales for multi-modal large language models,” in *Proceedings of European Conference on Computer Vision (ECCV)*, 2024.
- [27] W. Su, X. Zhu, Y. Cao, B. Li, L. Lu, F. Wei, and J. Dai, “Vl-bert: Pre-training of generic visual-linguistic representations,” in *Proceedings of International Conference on Learning Representations (ICLR)*, 2019.
- [28] J. Lu, D. Batra, D. Parikh, and S. Lee, “Vilbert: Pretraining task-agnostic visiolinguistic representations for vision-and-language tasks,” in *Proceedings of Advances in Neural Information Processing Systems (NeurIPS)*, 2019.
- [29] X. Li, X. Yin, C. Li, P. Zhang, X. Hu, L. Zhang, L. Wang, H. Hu, L. Dong, F. Wei, *et al.*, “Oscar: Object-semantics aligned pre-training for vision-language tasks,” in *Proceedings of European Conference on Computer Vision (ECCV)*, 2020.
- [30] Y.-C. Chen, L. Li, L. Yu, A. El Kholy, F. Ahmed, Z. Gan, Y. Cheng, and J. Liu, “Uniter: Universal image-text representation learning,” in *Proceedings of European Conference on Computer Vision (ECCV)*, 2020.

- [31] J. Lu, V. Goswami, M. Rohrbach, D. Parikh, and S. Lee, "12-in-1: Multi-task vision and language representation learning," in *Proceedings of Conference on Computer Vision and Pattern Recognition (CVPR)*, 2020.
- [32] S. Qian, W. Chen, M. Bai, X. Zhou, Z. Tu, and L. E. Li, "Affordancellm: Grounding affordance from vision language models," in *Proceedings of Conference on Computer Vision and Pattern Recognition (CVPR)*, 2024.
- [33] X. Wang, G. Chen, G. Qian, P. Gao, X.-Y. Wei, Y. Wang, Y. Tian, and W. Gao, "Large-scale multi-modal pre-trained models: A comprehensive survey," *Machine Intelligence Research*, vol. 20, no. 4, pp. 447–482, 2023.
- [34] K. Fang, F. Liu, P. Abbeel, and S. Levine, "Moka: Open-world robotic manipulation through mark-based visual prompting," *Robotics: Science and Systems (RSS)*, 2024.
- [35] T.-Y. Lin, M. Maire, S. Belongie, J. Hays, P. Perona, D. Ramanan, P. Dollár, and C. L. Zitnick, "Microsoft coco: Common objects in context," in *Proceedings of European Conference on Computer Vision (ECCV)*, 2014.
- [36] A. Gupta, P. Dollar, R. Girshick, K. He, P. Dollar, and R. Girshick, "Lvis: A dataset for large vocabulary instance segmentation," in *Proceedings of Conference on Computer Vision and Pattern Recognition (CVPR)*, 2019.
- [37] J. Xin, L. Wang, S. Wang, D. Kong, J. Li, and B. Yin, "A visual affordance reasoning network based on graph attention," in *International Conference on Digital Home (ICDH)*, 2022.
- [38] B. Zhou, H. Zhao, X. Puig, S. Fidler, A. Barriuso, and A. Torralba, "Scene parsing through ade20k dataset," in *Proceedings of Conference on Computer Vision and Pattern Recognition (CVPR)*, 2017.
- [39] C.-Y. Chuang, J. Li, A. Torralba, and S. Fidler, "Learning to act properly: Predicting and explaining affordances from images," in *Proceedings of Conference on Computer Vision and Pattern Recognition (CVPR)*, 2018.
- [40] J. Li, D. Li, C. Xiong, and S. Hoi, "Blip: Bootstrapping language-image pre-training for unified vision-language understanding and generation," in *Proceedings of International Conference on Machine Learning (ICML)*, 2022.
- [41] M. Deitke, D. Schwenk, J. Salvador, L. Weihs, O. Michel, E. VanderBilt, L. Schmidt, K. Ehsani, A. Kembhavi, and A. Farhadi, "Objaverse: A universe of annotated 3d objects," in *Proceedings of Conference on Computer Vision and Pattern Recognition (CVPR)*, 2023.
- [42] C. Li, R. Zhang, J. Wong, C. Gokmen, S. Srivastava, R. Martín-Martín, C. Wang, G. Levine, M. Lingelbach, J. Sun, *et al.*, "Behavior-1k: A benchmark for embodied ai with 1,000 everyday activities and realistic simulation," in *Conference on Robot Learning (CoRL)*, 2023.
- [43] A. Nguyen, D. Kanoulas, D. G. Caldwell, and N. G. Tsagarakis, "Detecting object affordances with convolutional neural networks," in *IEEE/RSJ International Conference on Intelligent Robots and Systems (IROS)*, 2016.
- [44] N. Friedman, D. Geiger, and M. Goldszmidt, "Bayesian network classifiers," *Machine Learning*, vol. 29, pp. 131–163, 1997.
- [45] W. S. Noble, "What is a support vector machine?," *Nature Biotechnology*, vol. 24, no. 12, pp. 1565–1567, 2006.
- [46] M. Lopes, F. S. Melo, and L. Montesano, "Affordance-based imitation learning in robots," in *IEEE/RSJ International Conference on Intelligent Robots and Systems (IROS)*, 2007.
- [47] L. Montesano, M. Lopes, A. Bernardino, and J. Santos-Victor, "Learning object affordances: from sensory–motor coordination to imitation," *IEEE Transactions on Robotics (T-RO)*, vol. 24, no. 1, pp. 15–26, 2008.
- [48] E. Uğur and E. Şahin, "Traversability: A case study for learning and perceiving affordances in robots," *Adaptive Behavior*, vol. 18, no. 3–4, pp. 258–284, 2010.
- [49] D. Chen, D. Kong, J. Li, S. Wang, and B. Yin, "A survey of visual affordance recognition based on deep learning," *IEEE Transactions on Big Data*, 2023.
- [50] T.-T. Do, A. Nguyen, and I. Reid, "Affordancenet: An end-to-end deep learning approach for object affordance detection," in *IEEE International Conference on Robotics and Automation (ICRA)*, 2018.
- [51] S. Levine, C. Finn, T. Darrell, and P. Abbeel, "End-to-end training of deep visuomotor policies," *Journal of Machine Learning Research (JMLR)*, vol. 17, no. 39, pp. 1–40, 2016.
- [52] S. Gupta, J. Davidson, S. Levine, R. Sukthankar, and J. Malik, "Cognitive mapping and planning for visual navigation," in *Proceedings of Conference on Computer Vision and Pattern Recognition (CVPR)*, 2017.
- [53] J. Sawatzky, Y. Sourli, C. Grund, and J. Gall, "What object should i use?—task driven object detection," in *Proceedings of Conference on Computer Vision and Pattern Recognition (CVPR)*, 2019.
- [54] Y. Zhu, A. Fathi, and L. Fei-Fei, "Reasoning about object affordances in a knowledge base representation," in *Proceedings of European Conference on Computer Vision (ECCV)*, 2014.
- [55] T. Nguyen, M. N. Vu, A. Vuong, D. Nguyen, T. Vo, N. Le, and A. Nguyen, "Open-vocabulary affordance detection in 3d point clouds," in *IEEE/RSJ International Conference on Intelligent Robots and Systems (IROS)*, 2023.
- [56] T. Van Vo, M. N. Vu, B. Huang, T. Nguyen, N. Le, T. Vo, and A. Nguyen, "Open-vocabulary affordance detection using knowledge distillation and text-point correlation," in *IEEE International Conference on Robotics and Automation (ICRA)*, 2024.
- [57] J. Wei, X. Wang, D. Schuurmans, M. Bosma, F. Xia, E. Chi, Q. V. Le, D. Zhou, *et al.*, "Chain-of-thought prompting elicits reasoning in large language models," in *Proceedings of Advances in Neural Information Processing Systems (NeurIPS)*, 2022.
- [58] C. Xu, Y. Chen, H. Wang, S.-C. Zhu, Y. Zhu, and S. Huang, "Partafford: Part-level affordance discovery from 3d objects," in *ECCV VOL1 Workshop*, 2022.
- [59] A. Myers, C. L. Teo, C. Fermüller, and Y. Aloimonos, "Affordance detection of tool parts from geometric features," in *IEEE International Conference on Robotics and Automation (ICRA)*, 2015.
- [60] H. Luo, W. Zhai, J. Zhang, Y. Cao, and D. Tao, "One-shot affordance detection," in *International Joint Conference on Artificial Intelligence (IJCAI)*, 2021.
- [61] L. Lu, W. Zhai, H. Luo, Y. Kang, and Y. Cao, "Phrase-based affordance detection via cyclic bilateral interaction," *IEEE Transactions on Artificial Intelligence*, vol. 4, no. 5, pp. 1186–1198, 2022.
- [62] W. Zhai, H. Luo, J. Zhang, Y. Cao, and D. Tao, "One-shot object affordance detection in the wild," *International Journal of Computer Vision (IJCV)*, vol. 130, no. 10, pp. 2472–2500, 2022.
- [63] T.-Y. Lin, M. Maire, S. Belongie, J. Hays, P. Perona, D. Ramanan, P. Dollár, and C. L. Zitnick, "Microsoft coco: Common objects in context," in *Proceedings of European Conference on Computer Vision (ECCV)*, 2014.
- [64] K. Ikeuchi and M. Hebert, "Task-oriented vision," in *Exploratory vision: the active eye*, pp. 257–277, Springer, 1996.
- [65] A. T. Miller, S. Knoop, H. I. Christensen, and P. K. Allen, "Automatic grasp planning using shape primitives," in *IEEE International Conference on Robotics and Automation (ICRA)*, 2003.
- [66] G. Vezzani, U. Pattacini, and L. Natale, "A grasping approach based on superquadratic models," in *IEEE International Conference on Robotics and Automation (ICRA)*, 2017.
- [67] D. Song, C. H. Ek, K. Huebner, and D. Kragic, "Task-based robot grasp planning using probabilistic inference," *IEEE Transactions on Robotics (T-RO)*, vol. 31, no. 3, pp. 546–561, 2015.
- [68] V. Narayanan and M. Likhachev, "Task-oriented planning for manipulating articulated mechanisms under model uncertainty," in *IEEE International Conference on Robotics and Automation (ICRA)*, 2015.
- [69] R. Gong, J. Huang, Y. Zhao, H. Geng, X. Gao, Q. Wu, W. Ai, Z. Zhou, D. Terzopoulos, S.-C. Zhu, *et al.*, "Arnold: A benchmark for language-grounded task learning with continuous states in realistic 3d scenes," in *Proceedings of International Conference on Computer Vision (ICCV)*, 2023.
- [70] S. James, Z. Ma, D. R. Arrojo, and A. J. Davison, "Rlbench: The robot learning benchmark & learning environment," *IEEE Robotics and Automation Letters (RA-L)*, vol. 5, no. 2, pp. 3019–3026, 2020.
- [71] Z. Xia, Z. Deng, B. Fang, Y. Yang, and F. Sun, "A review on sensory perception for dexterous robotic manipulation," *International Journal of Robotics Research (IJRR)*, vol. 19, no. 2, p. 17298806221095974, 2022.
- [72] A. Agarwal, S. Uppal, K. Shaw, and D. Pathak, "Dexterous functional grasping," in *Conference on Robot Learning (CoRL)*, 2023.
- [73] T. Zhu, R. Wu, J. Hang, X. Lin, and Y. Sun, "Toward human-like grasp: Functional grasp by dexterous robotic hand via object-hand semantic representation," *Transactions on Pattern Analysis and Machine Intelligence (TPAMI)*, vol. 45, no. 10, pp. 12521–12534, 2023.
- [74] C.-Y. Chuang, J. Li, A. Torralba, and S. Fidler, "Learning to act properly: Predicting and explaining affordances from images," in *Proceedings of Conference on Computer Vision and Pattern Recognition (CVPR)*, 2018.
- [75] H. W. Kuhn, "The hungarian method for the assignment problem," *Naval Research Logistics Quarterly*, vol. 2, no. 1–2, pp. 83–97, 1955.
- [76] H. Rezaatofghi, N. Tsoi, J. Gwak, A. Sadeghian, I. Reid, and S. Savarese, "Generalized intersection over union: A metric and a loss for bounding box regression," in *Proceedings of Conference on Computer Vision and Pattern Recognition (CVPR)*, 2019.
- [77] F. Milletari, N. Navab, and S.-A. Ahmadi, "V-net: Fully convolutional neural networks for volumetric medical image segmentation," in *International Conference on 3D Vision (3DV)*, 2016.
- [78] T.-Y. Lin, P. Goyal, R. Girshick, K. He, and P. Dollár, "Focal loss for dense object detection," in *Proceedings of International Conference on Computer Vision (ICCV)*, 2017.

- [79] S. Ren, K. He, R. Girshick, and J. Sun, "Faster r-cnn: Towards real-time object detection with region proposal networks," *Transactions on Pattern Analysis and Machine Intelligence (TPAMI)*, vol. 39, no. 6, pp. 1137–1149, 2016.
- [80] Y. Li, H. Mao, R. Girshick, and K. He, "Exploring plain vision transformer backbones for object detection," in *Proceedings of European Conference on Computer Vision (ECCV)*, 2022.
- [81] B. Sundaralingam, S. K. S. Hari, A. Fishman, C. Garrett, K. Van Wyk, V. Blukis, A. Millane, H. Oleynikova, A. Handa, F. Ramos, *et al.*, "Curobo: Parallelized collision-free robot motion generation," in *IEEE International Conference on Robotics and Automation (ICRA)*, IEEE, 2023.
- [82] H.-S. Fang, C. Wang, M. Gou, and C. Lu, "Graspnet-1billion: A large-scale benchmark for general object grasping," in *Proceedings of Conference on Computer Vision and Pattern Recognition (CVPR)*, 2020.
- [83] Y. Liu, "Roberta: A robustly optimized bert pretraining approach," *arXiv preprint arXiv:1907.11692*, vol. 364, 2019.
- [84] K. He, X. Zhang, S. Ren, and J. Sun, "Deep residual learning for image recognition," in *Proceedings of Conference on Computer Vision and Pattern Recognition (CVPR)*, 2016.
- [85] Y. Zhang, X. Huang, J. Ma, Z. Li, Z. Luo, Y. Xie, Y. Qin, T. Luo, Y. Li, S. Liu, *et al.*, "Recognize anything: A strong image tagging model," in *Proceedings of Conference on Computer Vision and Pattern Recognition (CVPR)*, 2024.
- [86] H. Zhang, F. Li, X. Zou, S. Liu, C. Li, J. Yang, and L. Zhang, "A simple framework for open-vocabulary segmentation and detection," in *Proceedings of International Conference on Computer Vision (ICCV)*, 2023.
- [87] N. Carion, F. Massa, G. Synnaeve, N. Usunier, A. Kirillov, and S. Zagoruyko, "End-to-end object detection with transformers," in *Proceedings of European Conference on Computer Vision (ECCV)*, 2020.
- [88] A. Kirillov, E. Mintun, N. Ravi, H. Mao, C. Rolland, L. Gustafson, T. Xiao, S. Whitehead, A. C. Berg, W.-Y. Lo, *et al.*, "Segment anything," in *Proceedings of Conference on Computer Vision and Pattern Recognition (CVPR)*, 2023.



Xiaomeng Zhu is a first-year Ph.D. student in the Department of Computer Science and Engineering at the Hong Kong University of Science and Technology. She received her B.Eng. degree in automation from the University of Electronic Science and Technology of China and her Master's degree in pattern recognition and intelligent systems from the Institute of Automation, Chinese Academy of Sciences. Her research focuses on advancing robotic understanding of human intent and environmental context to enable more effective human-robot collaboration.



Yuyang Li is a first-year PhD student at the Institute for AI, Peking University. He received his bachelor's degree in engineering from the Department of Automation at Tsinghua University in 2024. He aspires to advance the development of embodied intelligence, enabling machines to interpret multimodal sensory input, and interact with the environment with human-level adeptness.



Leiya Cui received his B.Eng. degree from the school of Information and Electronics at the Beijing Institute of Technology in 2024. He is now a first-year Ph.D. student at the Shenyang Institute of Automation, Chinese Academy of Sciences. He is also a research intern at the Institute for AI, Peking University. His research interest currently focuses on robot perception.



Pengfei Li is a third-year Ph.D. student at the Institute for AI Industry Research, Tsinghua University. He received the B.E. degree in Computer Science and Technology from University of Chinese Academy of Sciences, Beijing, China, in 2022. His research interests include autonomous driving and robotics.



Huan-ang Gao is a first-year PhD student at the Department of Computer Science and Technology and the Institute for AI Industry Research at Tsinghua University. He earned his bachelor's degree in engineering from the same department at Tsinghua University in 2024. His research focuses on developing generative simulation methods for evaluating and training embodied AI policies.



Yixin Zhu is an Assistant Professor and the Assistant Dean at the Institute for Artificial Intelligence, Peking University. He received a Ph.D. degree from UCLA in 2018, advised by Prof. Song-Chun Zhu. His research builds interactive AI by integrating high-level common sense (functionality, affordance, physics, causality, intent) with raw sensory inputs (pixels and haptic signals) to enable richer representation and cognitive reasoning on objects, scenes, shapes, numbers, and agents.



Hao Zhao received the B.E. degree and the Ph.D. degree both from the EE department of Tsinghua University, Beijing, China. He is currently an Assistant Professor with the Institute for AI Industry Research (AIR), Tsinghua University. He was a research scientist at Intel Labs China and a joint postdoc affiliated to Peking University. His research interests cover various computer vision topics related to robotics, especially 3D scene understanding. Photograph not available at the time of publication.

APPENDIX

A. Noun Features

In the context of visual input processing, a single image may contain zero or multiple objects capable of affording a particular task. When multiple objects are present, they may be distributed across different categorical classifications. The linguistic input \mathbf{X}_l , structured in verb-noun format, corresponds directly to the veridical object categories. Our implementation adopts the following protocol: For scenarios where the target count $n_{\text{gt}} = 0$, we employ a null string to construct \mathbf{X}_l . In instances where $n_{\text{gt}} > 0$ with uniform object categorization, we construct \mathbf{X}_l using a syntactic structure exemplified by “sit comfortably on sofa”. For cases where $n_{\text{gt}} > 0$ with heterogeneous object categories, \mathbf{X}_l is constructed through the concatenation of multiple verbal phrases, such as “sit comfortably on chair sit comfortably on bed”.

The memory bank modification protocol is exclusively activated for the latter two scenarios. In these instances, when the text encoder decomposes a noun into multiple tokenized features, we utilize the mean value of the transformer encoder-processed features as $l_{\text{noun}}^{\text{tr}}$ for updating purposes. In scenarios involving multiple categories, we compute $l_{\text{noun}}^{\text{tr}}$ as the arithmetic mean of the various noun features $l_{\text{noun}-1}^{\text{tr}}, \dots, l_{\text{noun}-n_c}^{\text{tr}}$, where n_c represents the category count. This computational approach facilitates the efficient transfer of privileged information from multiple nominal features to the student model’s singular pronoun feature, particularly in cases where an image contains multiple object classes equally suitable for task execution.

B. Loss Functions

We provide a detailed description of the loss terms used for plain Afford-X training. For each training sample, let \mathbf{O}_{gt} be its ground truth objects, and define $\mathbf{p}_i^{\text{span}} = [p_{i,1}^{\text{span}}, \dots, p_{i,n_{\text{max}}}^{\text{span}}] \in [0, 1]^{n_{\text{max}}}$ as a uniform distribution over the text-token span positions corresponding to the i -th ground truth object. The term $p_{i,n_{\text{max}}}^{\text{span}}$ signifies the probability of “no-object” and is 0 for genuine ground truth objects.

As a reminder, we treat the entire verb-pronoun (or verb-noun) expression as a token span. Suppose n_{gt} (the number of elements in \mathbf{O}_{gt}) is less than n_{pred} (the number of predicted objects \mathbf{O}_{pred}). We pad \mathbf{O}_{gt} with \emptyset (“no-object”) to match n_{pred} , calling the result \mathbf{O}'_{gt} . For any padded \emptyset , $\mathbf{p}_i^{\text{span}}$ is defined by $p_{i,j}^{\text{span}} = \mathbb{1}_{\{j=n_{\text{max}}\}}$, meaning $p_{i,n_{\text{max}}}^{\text{span}} = 1$ and 0 otherwise.

We denote the bipartite matching between \mathbf{O}'_{gt} and \mathbf{O}_{pred} as $\hat{\sigma}_0$, computed by minimizing the matching loss using the Hungarian algorithm [87]:

$$\hat{\sigma}_0 = \arg \min_{\sigma_0 \in \mathfrak{S}_{n_{\text{pred}}}} \sum_i^{n_{\text{pred}}} \mathbb{1}_{\{p_{i,n_{\text{max}}}^{\text{span}} = 0\}} \left[\mathcal{L}_{\text{ll}}(b_i, \hat{b}_{\sigma_0(i)}) + \mathcal{L}_{\text{giou}}(b_i, \hat{b}_{\sigma_0(i)}) + \mathcal{L}_{\text{token-m}}(\mathbf{p}_i^{\text{span}}, \hat{\mathbf{g}}_{\sigma_0(i)}) \right]. \quad (\text{A1})$$

Here, $\mathfrak{S}_{n_{\text{pred}}}$ indicates all permutations of n_{pred} elements. b_i and $\hat{b}_{\sigma_0(i)}$ refer to the ground truth and predicted boxes,

respectively, and $\hat{\mathbf{g}}_{\sigma_0(i)}$ is the predicted logit (detailed in the main paper). The losses are defined as follows:

$$\begin{aligned} \mathcal{L}_{\text{ll}}(b_i, \hat{b}_{\sigma_0(i)}) &= \|b_i - \hat{b}_{\sigma_0(i)}\|_1, \\ \mathcal{L}_{\text{giou}}(b_i, \hat{b}_{\sigma_0(i)}) &= 1 - \left(\frac{|b_i \cap \hat{b}_{\sigma_0(i)}|}{|b_i \cup \hat{b}_{\sigma_0(i)}|} - \frac{|B(b_i, \hat{b}_{\sigma_0(i)}) \setminus (b_i \cup \hat{b}_{\sigma_0(i)})|}{|B(b_i, \hat{b}_{\sigma_0(i)})|} \right), \quad (\text{A2}) \\ \mathcal{L}_{\text{token-m}}(\mathbf{p}_i^{\text{span}}, \hat{\mathbf{g}}_{\sigma_0(i)}) &= - \sum_j^{n_{\text{max}}} p_{i,j}^{\text{span}} \frac{\exp(\hat{g}_j^{\sigma_0(i)})}{\sum_{l=1}^{n_{\text{max}}} \exp(\hat{g}_l^{\sigma_0(i)})}. \end{aligned}$$

where $\mathcal{L}_{\text{giou}}$ is the Generalized Intersection over Union loss [76], and $|\cdot|$ denotes the area size. $B(b_i, \hat{b}_{\sigma_0(i)})$ is the smallest box containing both b_i and $\hat{b}_{\sigma_0(i)}$. Since $\mathcal{L}_{\text{giou}}$ is implemented by linear functions, it remains differentiable for backpropagation.

For segmentation, we employ Dice/F-1 loss [77] $\mathcal{L}_{\text{dice}}$ and Focal cross-entropy loss [78] $\mathcal{L}_{\text{cross}}$:

$$\mathcal{L}_{\text{dice}}(m_i, \hat{m}_{\sigma_0(i)}) = 1 - \frac{2m_i \delta(\hat{m}_{\sigma_0(i)}) + 1}{\delta(\hat{m}_{\sigma_0(i)}) + m_i + 1}, \quad (\text{A3})$$

where m_i is the ground truth mask for the i -th object, $\hat{m}_{\sigma_0(i)}$ denotes the predicted mask logits, and δ is the sigmoid function.

$$\mathcal{L}_{\text{cross}}(m_i, \hat{m}_{\sigma_0(i)}) = -\alpha_t (1 - p_t)^\gamma [m_i \log \delta(\hat{m}_{\sigma_0(i)}) + (1 - m_i) \log(1 - \delta(\hat{m}_{\sigma_0(i)}))], \quad (\text{A4})$$

$$\alpha_t = \alpha m_i + (1 - \alpha)(1 - m_i), \quad (\text{A5})$$

$$p_t = m_i \delta(\hat{m}_{\sigma_0(i)}) + (1 - m_i)(1 - \delta(\hat{m}_{\sigma_0(i)})).$$

Here, α and γ are hyper-parameters.

The soft-token prediction loss $\mathcal{L}_{\text{token}}$ is defined as:

$$\mathcal{L}_{\text{token}}(\mathbf{p}_i^{\text{span}}, \hat{\mathbf{g}}_{\sigma_0(i)}) = - \sum_j^{n_{\text{max}}} p_{i,j}^{\text{span}} \log \frac{\exp(\hat{g}_j^{\sigma_0(i)})}{\sum_{l=1}^{n_{\text{max}}} \exp(\hat{g}_l^{\sigma_0(i)})}. \quad (\text{A6})$$

The contrastive alignment loss encourages alignment between the embedded features of predicted objects and their corresponding text tokens. We project both the text features (processed by the transformer encoder) and the transformer decoder’s output features to the same smaller dimension, following [4]:

$$\begin{aligned} \mathcal{L}_{\text{align}} &= \frac{1}{2} \sum_i^{n_{\text{pred}}} \frac{1}{|T_i^+|} \sum_{j \in T_i^+} - \log \frac{\exp(o_i^\top t_j / \tau)}{\sum_{k=1}^{n_{\text{max}}} \exp(o_i^\top t_k / \tau)} \\ &\quad + \frac{1}{2} \sum_i^{n_{\text{max}}} \frac{1}{|O_i^+|} \sum_{j \in O_i^+} - \log \frac{\exp(t_i^\top o_j / \tau)}{\sum_{k=1}^{n_{\text{pred}}} \exp(t_i^\top o_k / \tau)}. \quad (\text{A7}) \end{aligned}$$

Here, T_i^+ is the set of token features to be aligned with a predicted object feature o_i , and O_i^+ is the set of object features aligned with a token feature t_i . We exclude any predicted object matched to \emptyset , and τ is a hyper-parameter.

Finally, the overall loss for plain Afford-X is:

$$\begin{aligned} \mathcal{L}_{\text{Afford-X}} &= \mathbb{1}_{\{p_{i,n_{\text{max}}}^{\text{span}} = 0\}} [\lambda_1 \mathcal{L}_{\text{ll}}(b_i, \hat{b}_{\sigma_0(i)}) + \lambda_2 \mathcal{L}_{\text{giou}}(b_i, \hat{b}_{\sigma_0(i)})] \\ &\quad + \mathbb{1}_{\{p_{i,n_{\text{max}}}^{\text{span}} = 0\}} [\lambda_3 \mathcal{L}_{\text{dice}}(m_i, \hat{m}_{\sigma_0(i)}) + \lambda_4 \mathcal{L}_{\text{cross}}(m_i, \hat{m}_{\sigma_0(i)})] \quad (\text{A8}) \\ &\quad + \lambda_5 \mathcal{L}_{\text{token}}(\mathbf{p}_i^{\text{span}}, \hat{\mathbf{g}}_{\sigma_0(i)}) + \lambda_6 \mathcal{L}_{\text{align}}. \end{aligned}$$

In this section, we present comprehensive qualitative evaluations across three datasets, comprising 14, 28, and 49 images respectively. Our experimental results demonstrate that the model achieves high precision in bounding box predictions across various scenarios. However, we observe that instance mask predictions occasionally exhibit suboptimal boundary adherence, particularly in regions with complex object con-

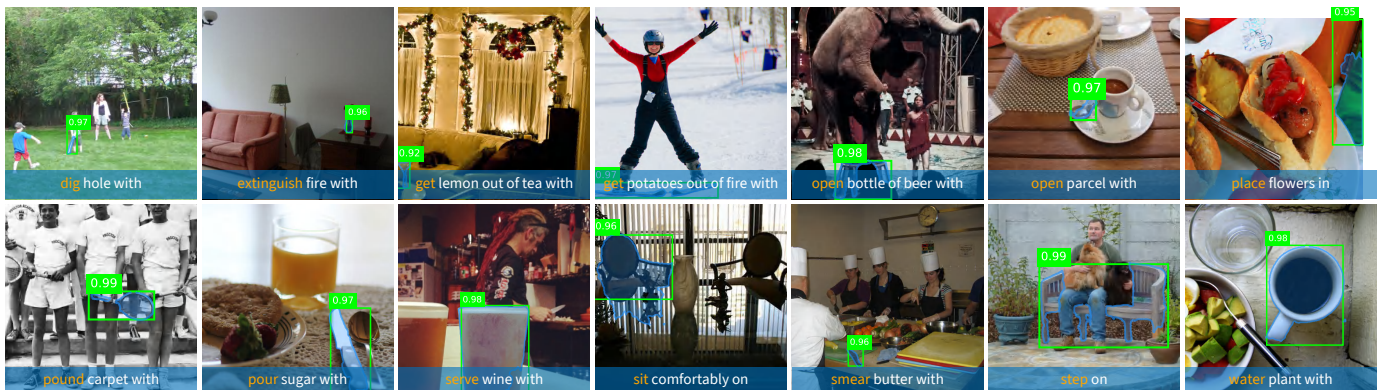


Fig. A1: Qualitative results on COCO-Tasks.

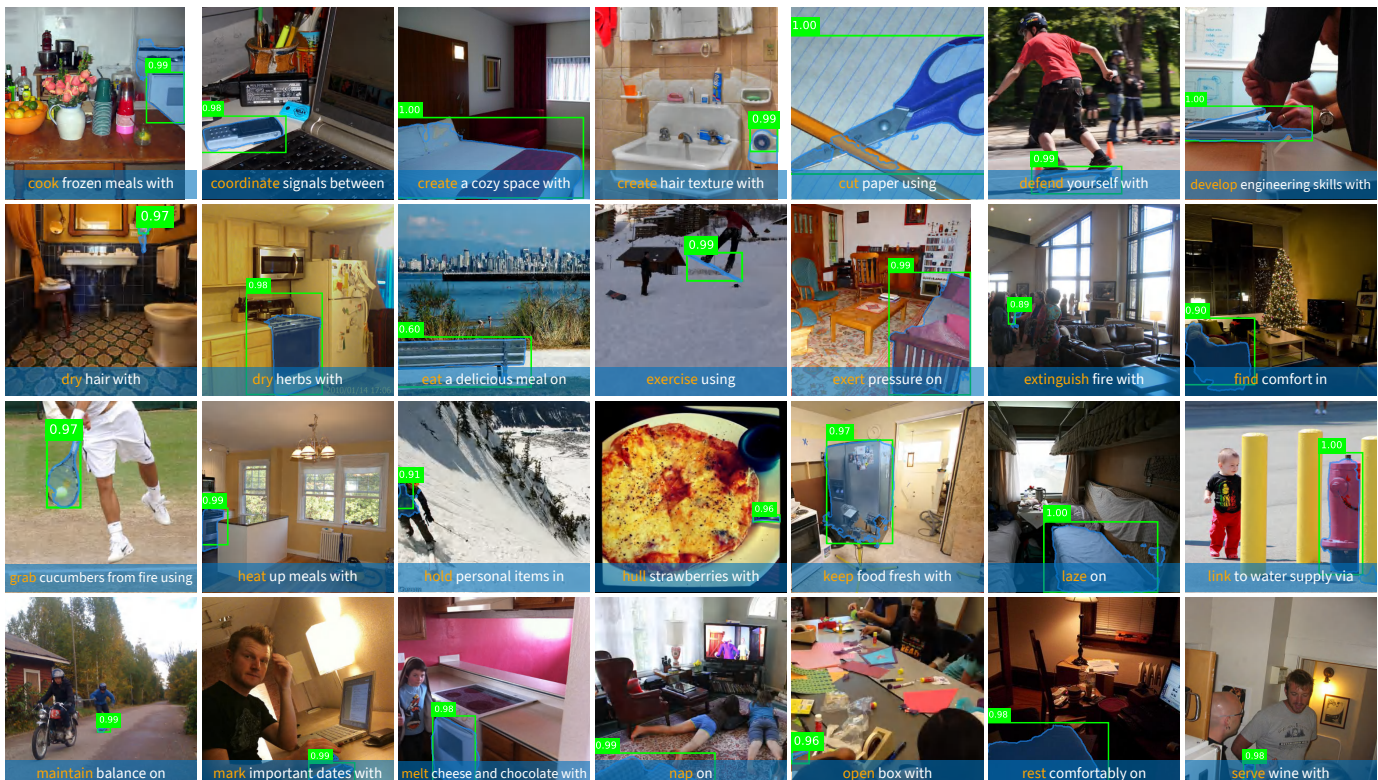


Fig. A2: Qualitative results on COCO-Aff.

tours. This limitation suggests potential for enhancement in mask refinement. As a promising future direction, we propose integrating the Segment Anything Model (SAM) [88] architecture to perform post-processing refinement of instance masks, which could potentially yield more precise object delineation and improved segmentation quality.

C. Visualization of Task-oriented Object Features

To evaluate the model’s ability to learn and focus on task-oriented physical properties from large-scale data, we visualized the attention maps produced by the last layer of the decoder (Fig. A4). In the “drink water with” task, the model emphasizes key parts of the container, indicating it effectively learns the physical properties relevant to that task. Furthermore, for the “sit comfortably on” task, the attention maps reveal that the model focuses on critical functional areas

such as the seat surface, backrest, and supporting structures of both the chair and bed. This suggests that our model has successfully learned to identify not just the objects themselves, but also their task-relevant physical attributes and affordances. The consistent high-confidence detection scores (ranging from 0.99 to 1.00) across different object categories demonstrate the model’s robust performance in identifying task-appropriate objects while maintaining awareness of their functional properties.

D. Ablation Study

Interaction of the Two Distillation Components: Tab. IV (d) and (f) compare the effects of cluster loss or cluster center replacement together with soft binary target loss. In (d), we observe +2.5% mAP^{box} and +3.4% mAP^{mask} , showing the synergy of these two distillation losses. By contrast, (f) shows



Fig. A3: Qualitative results on LVIS-Aff.

+1.0% mAP^{box} and +2.1% mAP^{mask} , still better than cluster loss alone (e), yet lower than soft binary target loss alone (b). These results indicate that preference distillation effectively improves object preference modeling, but simply replacing pronoun features to indicate target objects can diminish preference distillation effects if used in isolation.

Ablations for Pronoun Input:

Tab. A1 reports how using different pronouns in our baseline model and its distillation-augmented version (both trained on COCO-Tasks) affects performance. In either scenario, using *something*, *it*, or *them* yields similar results, whereas a random string (*abcd*) degrades performance slightly. Nevertheless,

the proposed distillation framework continues to work well, demonstrating its robustness.

Results Without Pre-training: Our architecture leverages pre-trained noun referring expression comprehension models. To verify that the noun-pronoun distillation framework itself is a standalone contribution, we run experiments from scratch on the COCO-Tasks dataset (see Tab. A2). Even without pre-training, the distillation mechanism still provides noticeable improvements.

Ablations for Task Number: Finally, Tab. A3 studies how different task numbers n_{task} influence performance on COCO-Tasks. The first row corresponds to our baseline model without distillation. Smaller n_{task} often yields better performance,

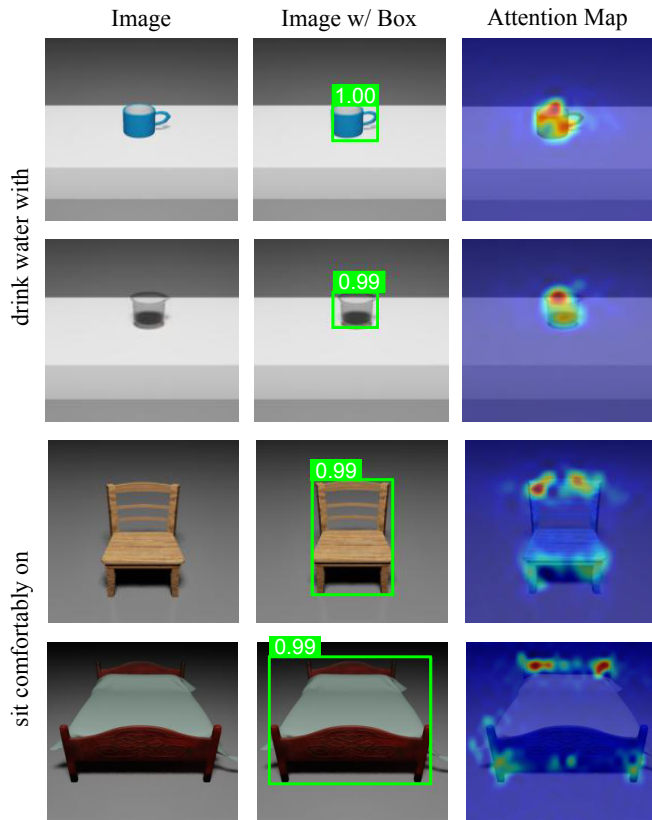


Fig. A4: **Attention map of selected results.** Each row shows the input image (left), detection results with confidence scores (middle), and corresponding attention maps (right). The images are organized to demonstrate the model’s ability to attend to task-relevant objects for two distinct actions: “drink water with” (top two rows) and “sit comfortably on” (bottom two rows).

TABLE A1: **Ablations for pronoun input on COCO-Tasks.**

Method	Pronoun	mAP ^{box}	mAP ^{mask}
baseline	something	41.3	35.2
	it	41.3	35.2
	them	41.4	35.0
	abcd	39.0	33.2
+ distillation	something	44.1	39.0
	it	43.8	38.4
	them	43.8	38.1
	abcd	42.8	37.4

TABLE A2: **Results without pre-training on COCO-Tasks.**

Method	mAP ^{box}	mAP ^{mask}
verb-pronoun input	3.65	5.74
verb-noun input	11.19	12.67
noun-pronoun distillation	7.43 (+3.78)	11.28 (+5.54)

likely because reduced task complexity makes it easier for the model to focus on verb understanding through noun-pronoun distillation.

E. Stability and Generalization under Larger-Scale Training Datasets

To examine how training on larger-scale datasets affects the model’s stability and generalization on a previously defined,

TABLE A3: **Ablations for the task number n_{task} on COCO-Tasks.**

Method	step on something	sit comfortably	place flowers	get potatoes out of fire
baseline	44.0	39.5	46.7	43.1
$n_{task} = 14$	46.2 (+2.2)	39.6 (+0.1)	49.9 (+3.2)	47.1 (+4.0)
$n_{task} = 5$	46.4 (+2.4)	40.7 (+1.2)	51.3 (+4.6)	46.8 (+3.7)
$n_{task} = 1$	47.0 (+3.0)	42.1 (+2.6)	50.8 (+4.1)	47.4 (+4.3)

TABLE A4: **Performance Analysis Across Training Datasets and Text Input Configurations.** Evaluation metrics (mAP^{box} and mAP^{mask}) reported for both training datasets and COCO-Tasks. Results demonstrate the effects of scaling task sets and object categories on transfer performance. Input configurations including VP: verb-pronoun, VN: verb-noun, and D: noun-pronoun distillation.

Training Data.	Input	Test on Training Data.		Test on COCO-Tasks	
		mAP ^{box}	mAP ^{mask}	mAP ^{box}	mAP ^{mask}
COCO-Tasks	VP	43.2	36.9	—	—
	VN	54.8	47.5	—	—
	D	45.3	39.2	—	—
COCO-Aff	VP	45.2	41.4	42.7	38.1
	VN	48.8	44.5	54.5	46.1
	D	45.8	42.5	43.9	38.3
LVIS-Aff	VP	26.8	24.2	29.5	25.8
	VN	33.8	35.1	32.0	28.6
	D	27.7	24.8	27.8	25.3

task-specific benchmark, we conducted a series of experiments. We trained our model on three datasets of increasing complexity: from the original COCO-Tasks dataset (14 tasks), to COCO-Aff (1,144 tasks and 80 object categories), and finally the more extensive LVIS-Aff (1,494 tasks and 1,064 categories). The model was subsequently evaluated on the COCO-Tasks benchmark.

As shown in Tab. A4, when trained on COCO-Aff, the model’s performance on COCO-Tasks remained close to the baseline established by direct training on COCO-Tasks. For instance, under a specific input configuration, the model achieved approximately 45.3% mAP^{box} when both trained and tested on COCO-Tasks. After training on COCO-Aff, the mAP^{box} dropped only slightly to around 43%-44%. This result suggests that although increasing the number of tasks and categories introduces greater complexity, it does not markedly degrade the model’s detection and segmentation performance on the original, task-specific benchmark.

F. Statistical Significance Analysis of LLM-based Baselines

Based on the one-tailed t-test results presented in Table Tab. A5, we observe statistically significant differences in performance between Afford-X and various LLM-based approaches. The table presents p-values for both precision and recall metrics, comparing against our COCO-Aff and LVIS-Aff trained frameworks.

For approaches employing detection before reasoning (rows (a) and (b)), we observe extremely low p-values ($p < 10^{-5}$) across all comparisons, indicating strong statistical significance in the performance differences. This aligns with our earlier observations regarding the limitations of LLM-based label reasoning, particularly in scenarios involving semantic ambiguity.

TABLE A5: **Statistical significance analysis.** Statistical significance analysis using one-tailed t-tests between our framework and various LLM-based approaches. Results demonstrate significant performance differences across different architectural approaches, particularly with traditional detection-first methods and end-to-end MLLM systems.

Index	Method	Precision		Recall	
		vs COCO-Aff	vs LVIS-Aff	vs COCO-Aff	vs LVIS-Aff
(a)	Detection + GPT4	3.21×10^{-11}	2.80×10^{-18}	5.09×10^{-11}	1.72×10^{-44}
(b)	Detection + BLIP + GPT4	3.68×10^{-6}	3.12×10^{-10}	5.44×10^{-6}	1.43×10^{-15}
(c)	GPT4 + OpenSeeD	3.70×10^{-3}	8.38×10^{-6}	8.33×10^{-3}	1.18×10^{-10}
(d)	GPT4V + OpenSeeD	1.86×10^{-1}	3.05×10^{-3}	8.74×10^{-2}	2.84×10^{-11}
(e)	SPHINX + OpenSeeD	6.21×10^{-1}	3.64×10^{-1}	2.46×10^{-1}	9.32×10^{-10}
(f)	SPHINX (CoT)	1.56×10^{-5}	3.89×10^{-10}	4.78×10^{-3}	9.71×10^{-11}

TABLE A6: Success rate (%) of each object selection across six different scene configurations. Each task was tested five times per scene.

Task	Coffee Table	Conference. Table	Counter-top 1	Counter-top 2	Desk	Shelf
clean electronic screens	20.0	50.0	40.0	40.0	80.0	40.0
drink water	100.0	100.0	100.0	80.0	100.0	100.0
protect items from rain	60.0	40.0	60.0	80.0	100.0	60.0
spread butter	100.0	85.71	100.0	80.0	80.0	80.0
stream video	100.0	100.0	100.0	100.0	80.0	100.0

The methods implementing reasoning before detection (rows (c), (d), and (e)) show an interesting progression in statistical significance. While GPT4 + OpenSeeD maintains strong significance levels ($p < 10^{-3}$ for most metrics), the GPT4V + OpenSeeD and SPHINX + OpenSeeD combinations show decreasing levels of statistical significance, particularly when compared against COCO-Aff ($p = 1.86 \times 10^{-1}$ and $p = 6.21 \times 10^{-1}$ for precision, respectively). This suggests that the integration of MLLM significantly enhances the model’s understanding of object geometry. This improvement helps to mitigate information asymmetry issues that can arise from combining functional modules. However, despite these advancements, the performance of these two pipelines still falls short compared to end-to-end approaches. This indicates that end-to-end MMs still possess certain advantages in affordance reasoning.

Additionally, we attempted to construct a baseline composed entirely of MLLM. Constrained by GPU limitations (24GB 3090), we employed SPHINX (1.1B) for this task. During experimentation, we found that due to its limited parameter count, the pipeline struggled to directly execute affordance reasoning instructions. Consequently, we implemented a two-stage chain of thought approach, where SPHINX first identifies objects in the scene before determining their functions. Results reveal significant performance variations across datasets. On COCO-Aff, SPHINX (CoT) showed statistically significant differences in both precision ($p = 1.56 \times 10^{-5}$) and recall ($p = 4.78 \times 10^{-3}$) compared to our framework. This gap widened on LVIS-Aff, with p-values reaching 3.89×10^{-10} for precision and 9.71×10^{-11} for recall. These findings suggest that pure MLLM approaches exhibit lower parameter efficiency compared to MM-based methods in addressing affordance reasoning tasks, while also highlighting the persistent challenges in solving visual problems entirely within the language space.

G. Embodied Affordance Reasoning

The virtual environments consist of 6 selected interior room layouts from the Evermotion dataset¹ and OmniGibson [42], with textured object meshes from Objaverse [41] placed in the scene.

1) *Affordance Reasoning in Scenes:* For evaluating the affordance reasoning capabilities of Afford-X in the scene, simulating an embodied perspective of robots, we evaluate the model with 6 common tasks in 6 different interior scenes. The evaluation pipeline follows Sec. VI-E. To create the cluttered scene in the real world, each problem instance now consists of 2 positive and 3 negative object categories sampled according to the dataset. One textured mesh for each selected category is sampled and loaded to a table in the interior scene in a random position, and we then run a few-step optimization to eliminate the inter-object penetration according to their 3D bounding boxes to ensure stable simulation and perception. A camera looking at the center of the table renders an RGB image with auxiliary bounding boxes exported for each object for evaluating the selection of Afford-X. 5 random samples with different objects and their layouts are generated for each of the 50 tasks and each of the 6 scenes for evaluation.

For each image, Afford-X is queried with the rendered image and the corresponding textual description for the task, and the output bounding box is compared with the ones exported from the simulation. Compared to the experiment settings in Sec. VI-E, more objects are randomly placed on the table to simulate the cluttered scenes in the real world. The perception of the scene, in addition to the objects, also provides distractions to the model, making the evaluation more challenging.

The experimental results presented in Tab. A6 and visualized in Fig. A6 demonstrate varying levels of performance across six distinct tasks, each evaluated through five trials in six different scene configurations. Statistical analysis demonstrates robust performance with a mean success

¹<https://evermotion.org/>

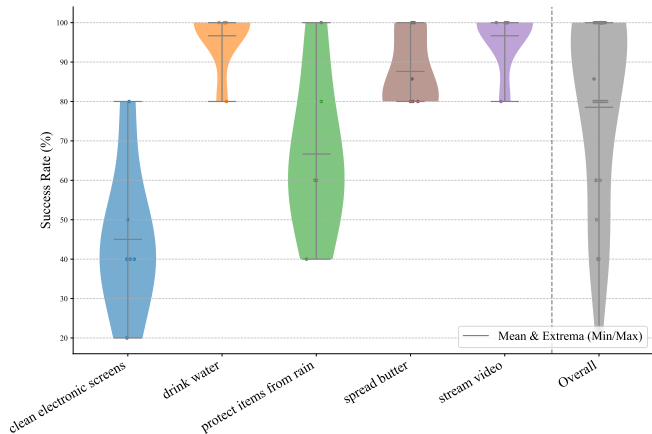


Fig. A6: **Success rate of object selections.** Each task was tested five times across six different scenes. Each point in the figure represents the average result for one scene.

rate of 80.44% ($\pm 3.5\%$) across all experimental conditions, providing empirical validation of our model’s effectiveness in dynamic, unconstrained environments. Statistical significance testing ($p < 0.01$) confirms the reliability of these findings, demonstrating that our affordance reasoning framework substantially enhances real-time decision-making capabilities and

operational efficiency. A more detailed evaluation compared to LLM-based pipelines and the corresponding analysis will be discussed in Sec. VI-E.

2) *Preference on Multiple Options:* To rigorously evaluate the model’s adaptive capabilities, we designed a progressive object selection test. In this setup, we systematically removed the robot’s preferred object choices for specific tasks, forcing it to identify and select alternative solutions. The experimental configuration (Fig. 13a) involved placing six candidate objects on a large table in an interior scene, including three positive object categories (e.g., “prepare drinks with” or “lay comfortably on”). Following each successful object selection, we removed the chosen object and observed the model’s subsequent adaptation strategies.

The results show that in all three task scenarios, Afford-X successfully selected objects that met the task requirements, with its selection process demonstrating a reasonable degree of preference. For example, in the task “prepare drinks with,” Afford-X first selected a blender, which is primarily used for making drinks, followed by a larger container (a pitcher), and finally a mug for serving the drink. This selection order indicates that for this task, Afford-X tends to prioritize objects with core functionality or larger capacity. In the task “lay com-

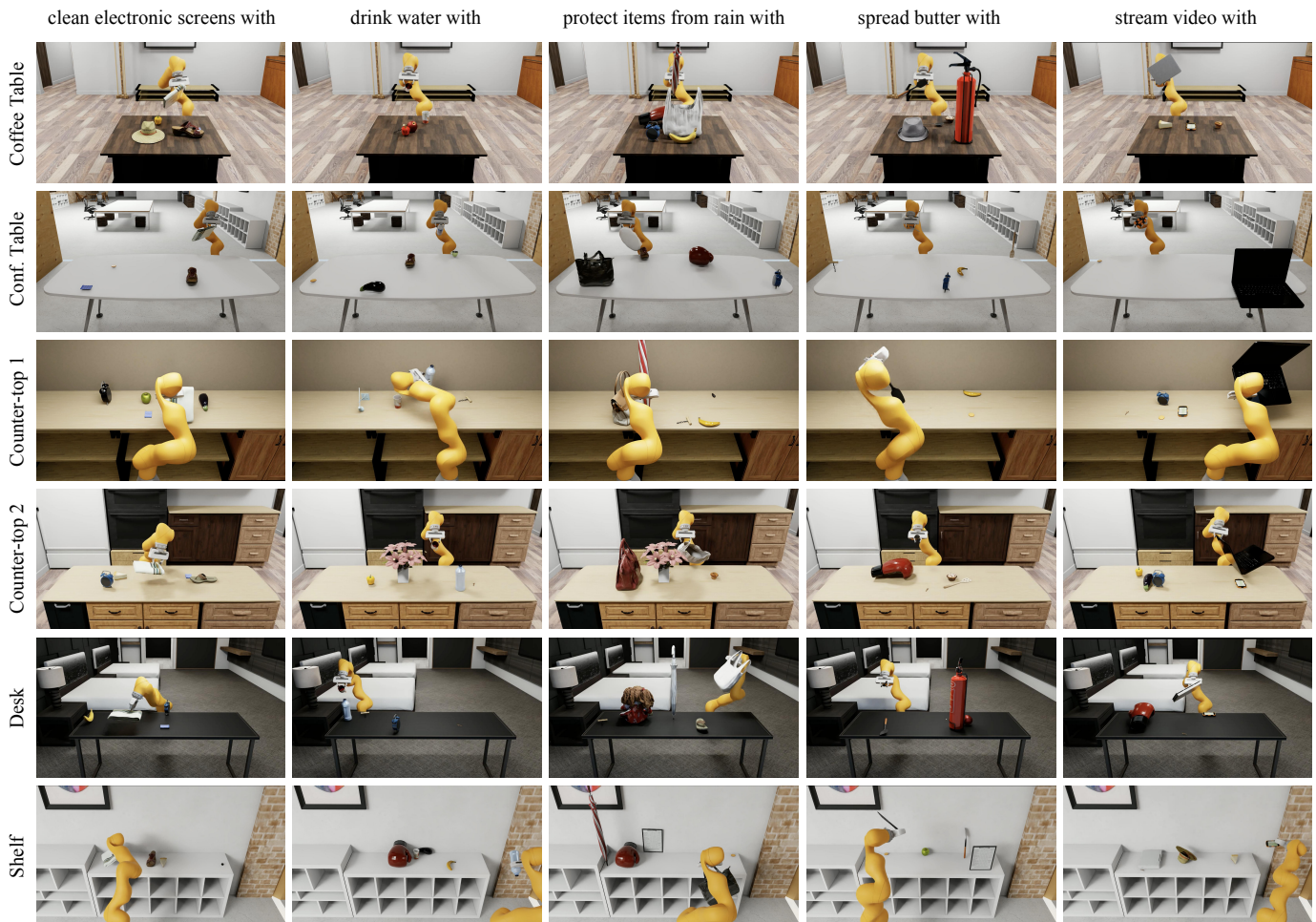


Fig. A5: **Task-oriented manipulation in simulated environments.** The robotic system integrated with Afford-X demonstrates versatile task-oriented manipulation capabilities across diverse simulated environments, successfully executing multiple affordance-based tasks in varying spatial and object configurations.

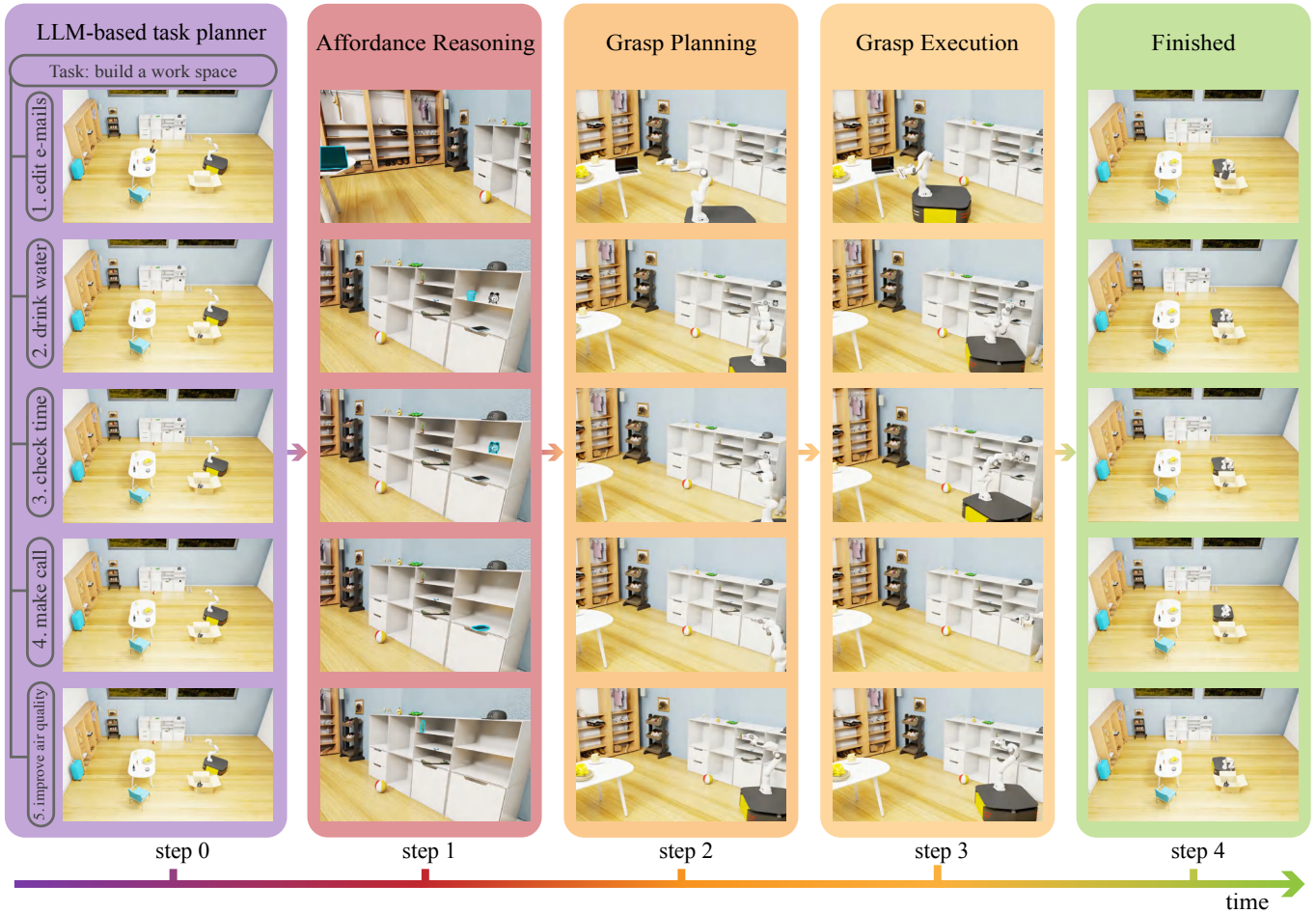


Fig. A7: **Results of the long-horizon task.** The system integrated with Afford-X demonstrates the potential to accomplish long-horizon tasks with the inclusion of an language-guided task planner. The task planner analyzes the user-specified long-horizon task and decomposes it into multiple short-term tasks. In the simulation environment, the robot performs task-oriented manipulation based on each of the subtasks.

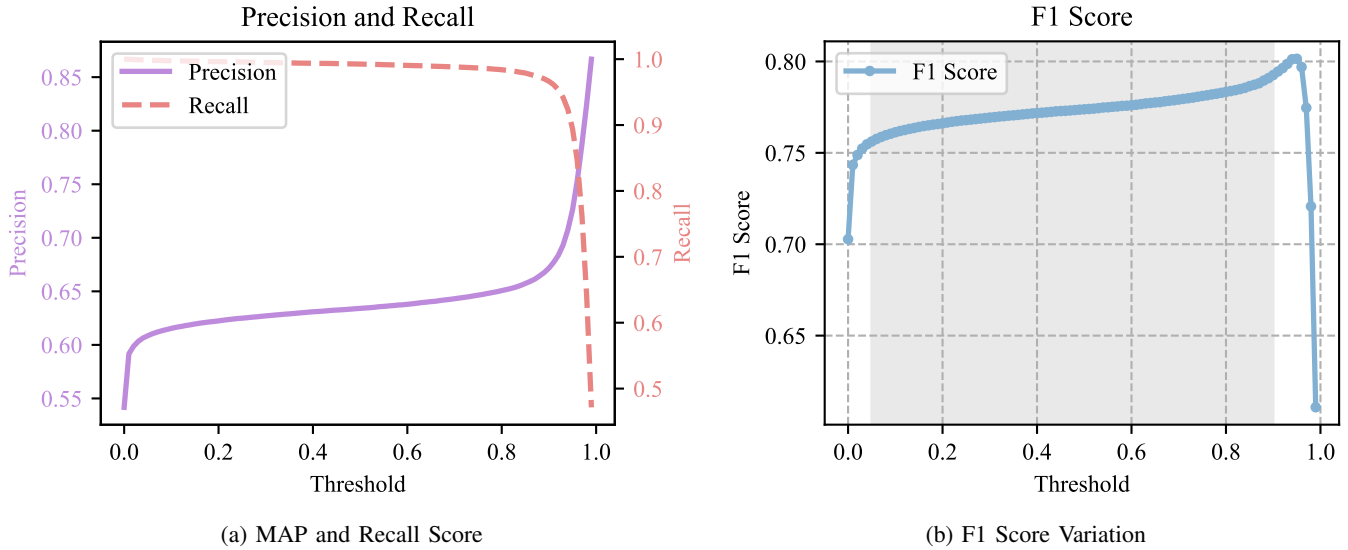
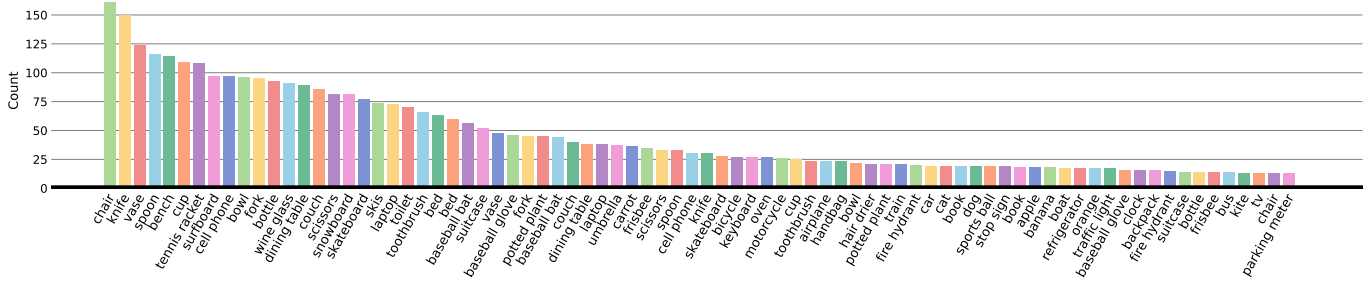
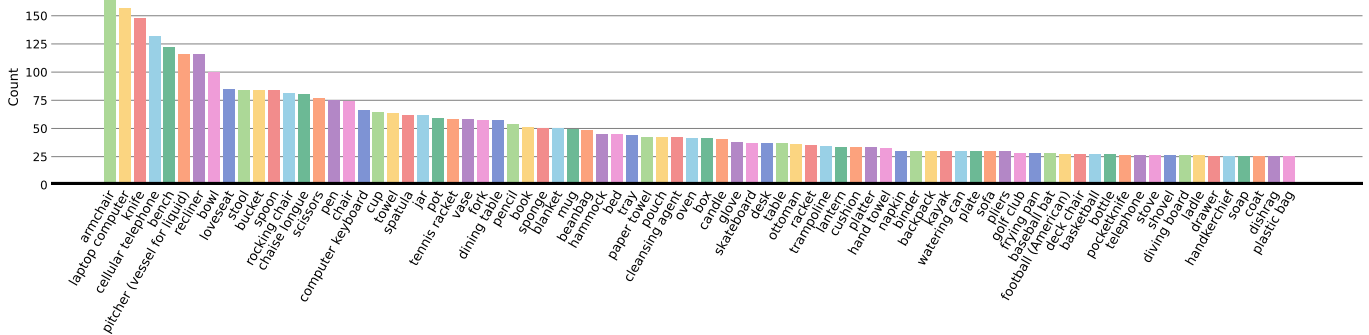


Fig. A8: The influence of different score threshold settings on test results: (a) The fluctuation curve of MAP and recall with the score threshold; (b) The F1 score evaluated the influence of different thresholds on the detection results.

fortably on,” Afford-X first selected a lounge, which appeared more comfortable for lying down, followed by a chair. This suggests that the model makes task-oriented selections based on both functional attributes and the appearance of the objects.



(a) The category frequency of objects in the COCO-Aff dataset.



(b) The category frequency of objects in the LVIS-Aff dataset.



(c) The word cloud of action labels for COCO-Aff.

(d) The word cloud of action labels for LVIS-Aff.

Fig. A9: Visualizations of COCO-Aff and LVIS-Aff datasets, including verb word clouds, partial task displays, and category frequencies.

H. Long Horizon Tasks

To evaluate the model’s capability in managing complex, multi-step operations, we integrated Afford-X with a language-guided task planner to address sophisticated objectives such as “*build a workspace task.*” As illustrated in Fig. A7, this integration enables hierarchical task decomposition, where the high-level planner breaks down complex goals into manageable subtasks, each requiring specific object selection and manipulation sequences. These subtasks are designed to align with the available objects and interaction possibilities in our dataset, ensuring compatibility with our manipulation pipeline. Our system successfully executes these subtasks through precise object detection, grasping, and placement operations, coordinating actions to achieve the overall objective.

This integrated approach demonstrates Afford-X’s effectiveness within a comprehensive decision-making framework, successfully combining sophisticated affordance reasoning with advanced language models to address complex, strategic objectives. The system’s ability to seamlessly bridge high-

level task decomposition with precise affordance-based object selection underscores its potential for real-world robotic applications, where success depends on both functional versatility and strategic planning capabilities. These results validate our model’s readiness for deployment in complex operational environments requiring both tactical adaptability and strategic coordination.

I. Threshold Selection Strategy

The selection of an acceptance threshold for outcomes is crucial for flexibility in choosing objects capable of undertaking a task. A lower threshold undoubtedly increases the likelihood of obtaining results but also significantly elevates the proportion of ineffective detection. Therefore, we experimented with various thresholds to identify a range that balances the probability of obtaining results and the proportion of valid outcomes. We employed recall and accuracy to measure these metrics, respectively, and used the harmonic mean of both, calculated as the F1 score, as a comprehensive evaluation criterion. The experimental results, depicted in

Fig. A8, demonstrate that as the acceptance threshold for detection scores increases, recall exhibits a sharp decline around a threshold of 0.9, while the accuracy curve surges abruptly. This indicates that a threshold of 0.9 represents a neutral choice, managing to balance the likelihood of obtaining results while enhancing the credibility of outcomes, as also evidenced in Fig. A8b. When the threshold is less than 0.05, both the accuracy curve and the F1 score curve show a steep downward trend, indicating a higher proportion of ineffective results in the detection outcomes. Overall, setting the threshold at 0.9 is identified as the optimal choice that balances the probability of obtaining results and the proportion of valid outcomes. Within the range of 0.05 to 0.9, the final threshold value can be flexibly determined based on the desired level of detection result flexibility.

J. Statistics

We provide more detailed statistics about our dataset, COCO-Aff and LVIS-Aff. The category frequency of encompassed objects in the dataset are visualized in Figs. A9a and A9b, and the word clouds of verbs related to affordances are illustrated in Figs. A9c and A9d. This enlarged dataset fulfills most affordance needs in daily life scenarios, shows strong open-set ability, and exhibits robust generalizability across unfamiliar task categories.

Additionally, Figs. A10a and A10b present a selection of tasks from the datasets, and Figs. A10c and A10d show the frequency distributions of object categories and verbs, limited to the top 20 object categories and top 80 verbs, respectively. It is evident that common household items such as “chairs,” “knives,” and “bowls” appear most frequently in both datasets.

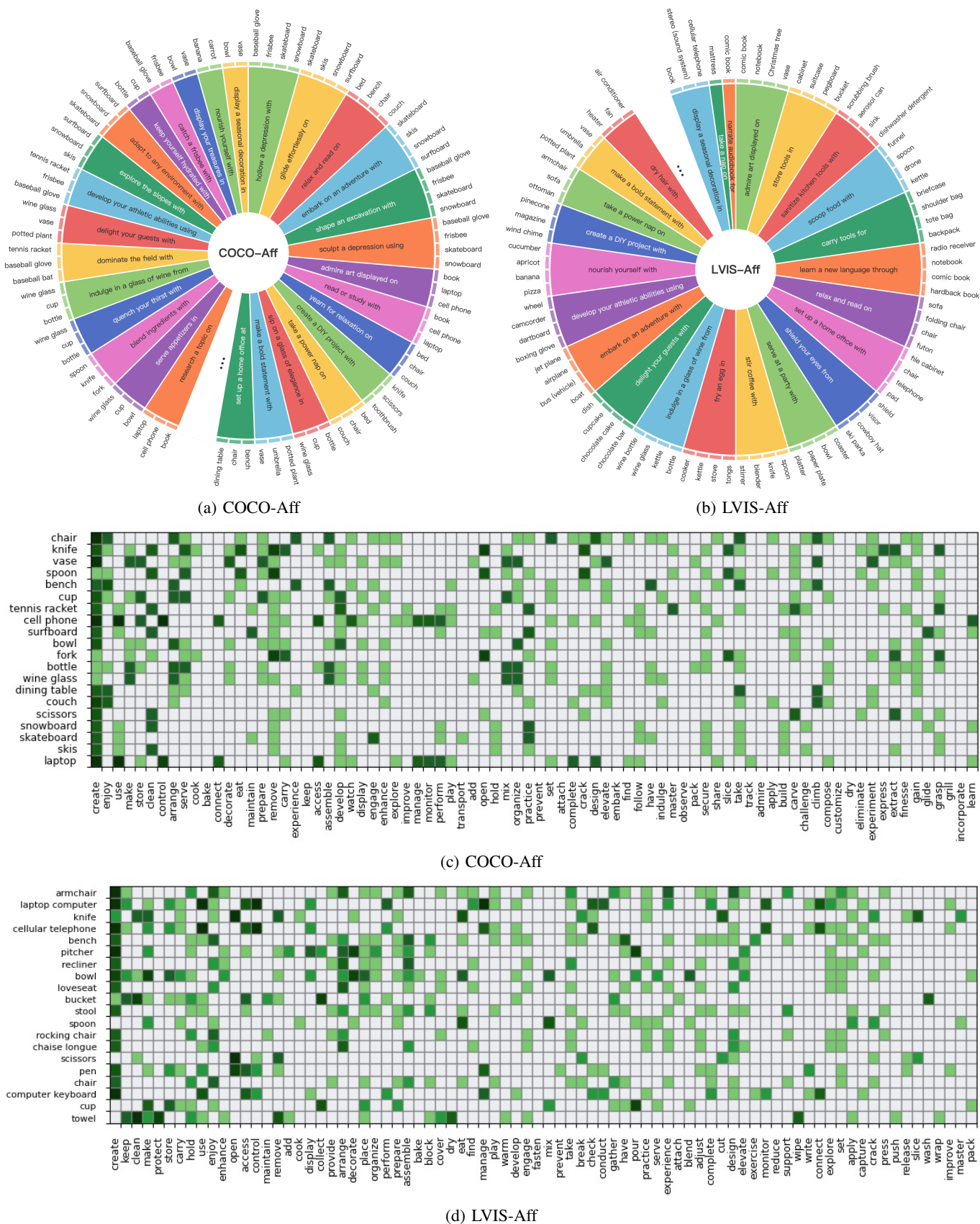


Fig. A10: Visualizations of COCO-Aff and LVIS-Aff datasets. (a-b) Sunburst charts demonstrate task visualizations for COCO-Aff and LVIS-Aff datasets. The inner ring shows actions while the outer ring displays corresponding objects, illustrating how various items are associated with daily activities. (c-d) The grid visualizations illustrate the frequency distributions of nouns across different verbs on COCO-Aff and LVIS-Aff datasets. Darker colors indicate higher frequencies, while lighter colors represent lower frequencies.